THE JOURNAL OF BIOLOGICAL CHEMISTRY VOL. 284, NO. 42, pp. 29050–29064, October 16, 2009

A Novel Signaling Pathway

FIBROBLAST NICOTINIC RECEPTOR α1 BINDS UROKINASE AND PROMOTES RENAL FIBROSIS[*S]

Received for publication, April 17, 2009 Published, JBC Papers in Press, August 18, 2009, DOI 10.1074/jbc.M109.010249

Guoqiang Zhang[‡1], Kelly A. Kernan[‡], Alison Thomas[‡], Sarah Collins[‡], Yumei Song[§], Ling Li[¶], Weizhong Zhu[‖], Renee C. LeBoeuf[**], and Allison A. Eddy[‡]

From the [‡]Division of Nephrology and [§]Division of Immunology, Seattle Children's Hospital Research Institute, Seattle, Washington 98101, the [‖]Department of Pathology and [**]Division of Endocrine and Metabolic Diseases, Department of Medicine, University of Washington, Seattle, Washington 98105, and the [¶]Seattle Biomedical Research Institute, Seattle, Washington 98101

The nicotinic acetylcholine receptor α1 (nAChRα1) was investigated as a potential fibrogenic molecule in the kidney, given reports that it may be an alternative urokinase (urokinase plasminogen activator; uPA) receptor in addition to the classical receptor uPAR. In a mouse obstructive uropathy model of chronic kidney disease, interstitial fibroblasts were identified as the primary cell type that bears nAChRα1 during fibrogenesis. Silencing of the nAChRα1 gene led to significantly fewer interstitial αSMA$^+$ myofibroblasts (2.8 times decreased), reduced interstitial cell proliferation (2.6 times decreased), better tubular cell preservation (E-cadherin 14 times increased), and reduced fibrosis severity (24% decrease in total collagen). The myofibroblast-inhibiting effect of nAChRα1 silencing in uPA-sufficient mice disappeared in uPA-null mice, suggesting that a uPA-dependent fibroblastic nAChRα1 pathway promotes renal fibrosis. To further establish this possible ligand-receptor relationship and to identify downstream signaling pathways, *in vitro* studies were performed using primary cultures of renal fibroblasts. ^{35}S-Labeled uPA bound to nAChRα1 with a K_d of 1.6 × 10^{-8} M, which was displaced by the specific nAChRα1 inhibitor D-tubocurarine in a dose-dependent manner. Pre-exposure of uPA to the fibroblasts inhibited [^{3}H]nicotine binding. The uPA binding induced a cellular calcium influx and an inward membrane current that was entirely prevented by D-tubocurarine preincubation or nAChRα1 silencing. By mass spectrometry phosphoproteome analyses, uPA stimulation phosphorylated nAChRα1 and a complex of signaling proteins, including calcium-binding proteins, cytoskeletal proteins, and a nucleoprotein. This signaling pathway appears to regulate the expression of a group of genes that transform renal fibroblasts into more active myofibroblasts characterized by enhanced proliferation and contractility. This new fibrosis-promoting pathway may also be relevant to disorders that extend beyond chronic kidney disease.

Urokinase was first isolated from human urine in 1955 and identified as an activator of plasminogen (urokinase plasminogen activator (uPA)[2]) (1). This serine protease is abundantly produced by kidney tubular cells and secreted across the apical membrane into the urinary space. Other cellular sources include monocytes/macrophages, fibroblasts, and myofibroblasts (2). Despite high uPA levels, its primary physiological function in the kidney remains unknown. Suggested roles have been an inhibitor of kidney stone formation and urinary tract infections due to its proteolytic activity and endogenous antibiotic function, respectively (3, 4). Increased uPA activity has been reported in several pathological conditions, such as chronic kidney disease (2), atherosclerosis, and malignant tumors (5, 6). Endogenous plasma uPA levels may be elevated 2–4-fold in patients with chronic kidney disease due to increased uPA released from damaged kidneys (7, 8).

Since its identification as a mediator of fibrin/fibrinogen degradation, uPA has been used in clinical settings as a fibrinolytic agent. The classical cellular urokinase receptor (uPAR) was first discovered on the surface of monocytes in 1985. Since then, a diverse array of biological functions triggered by uPA-uPAR interactions has been elucidated and shown to have important effects on cellular behavior during embryogenesis, angiogenesis, wound healing, and metastases (9–11). The specific role of uPA in fibrotic disorders appears to be organ-specific. uPA deficiency worsened bleomycin-induced lung fibrosis and reduced fibrosis in hearts damaged by viral myocarditis or left ventricular pressure overload, whereas there was no net effect on the severity of renal fibrosis induced by ureteral obstruction (UUO), although uPAR deficiency worsened fibrosis in that model (2). Despite its association with a broad repertoire of activities, the uPA mechanism of action remains incompletely understood. In particular, there is accumulating evidence that uPA may have protease- and uPAR-independent cellular effects. For example, macrophage uPA overexpression causes

* This work was supported, in whole or in part, by National Institutes of Health Grants DK54500 and DK44757 (to A. A. E.). This work was also supported by a scientist development grant from the American Heart Association National Center (to G. Z.) and the Young Investigator Award from Seattle Children's Hospital and Regional Medical Center (to G. Z.).

[S] The on-line version of this article (available at http://www.jbc.org) contains supplemental Tables S1 and S2 and Figs. S1–S3.

[1] To whom correspondence should be addressed: C9S, 1900 9th Ave., Seattle, WA 98101. Fax: 206-987-7660; E-mail: guoqiang.zhang@seattlechildrens.org.

[2] The abbreviations used are: uPA, urokinase plasminogen activator; uPAR, uPA receptor; nAChR, nicotinic acetylcholine receptor; UUO, unilateral ureteral obstruction; αSMA, α-smooth muscle actin; IP, immunoprecipitation; PCNA, proliferating cell nuclear antigen; ATF, amino terminal uPA fragment; ANOVA, analysis of variance; αBTx, α-bungarotoxin; *d*-TC, D-tubocurarine; neoN, neonicotine; siRNA, small interfering RNA; WT, wild type; DMEM, Dulbecco's modified Eagle's medium; IB, immunoblot; BrdUrd, bromodeoxyuridine; SFM, serum-free medium; IHC, immunohistochemical; ACh, acetylcholine.

cardiac inflammation and fibrosis. Of particular note, this effect is independent of the classic uPA receptor uPAR and can be abrogated using a calcium channel blocker (12).

Recent evidence suggests that additional uPA receptor(s) may exist (13–15). We reported that urokinase initiates renal fibroblast signaling via the MAPK/ERK pathway (16). This response appears to be mediated, at least in part, by an alternative urokinase receptor, since uPA can initiate mitogenesis in $uPAR^{-/-}$ fibroblasts. Using phage display technology, Liang *et al.* (17) reported putative uPA-binding consensus sequences in 12 transmembrane receptors and suggested them as candidate alternative uPA receptor(s). Of these candidate receptors, several are already known as uPAR co-receptors: low density lipoprotein receptor-related protein, gp130, integrin αv, uPAR-associated protein (also known as Endo180 and Mrc2), and the insulin-like growth factor II/mannose 6-phosphate receptor. It is also possible that different uPA domains might simultaneously bind to uPAR and one of its co-receptors (18). The muscle type nicotinic receptor α1 (nAChRα1) was among the receptor candidates. The muscle type nAChR is a ligand-gated ion channel known to mediate signal transduction at the neuromuscular junction (19). This receptor is a pentametric glycoprotein comprising five membrane-spanning subunits (two α1, β1, γ, and δ) that form a ligand-gated ion channel. The currently known nAChRα1 ligands are nicotine and acetylcholine. The ligand-binding domain (interface of α1/γ or α1/δ) involves the two α1 chains, which form a specialized pocket of aromatic and hydrophobic residues structurally similar to uPAR (20, 21). Upon ligation, the receptor changes its conformation and becomes permeable to sodium and calcium ions. Receptor function is regulated by tyrosine phosphorylation and dephosphorylation by kinases and phosphatases, respectively (22). The nAChRα1 is expressed and activated during muscle differentiation during embryonic development and following mature muscle denervation (23). Vascular endothelium, macrophages, and fibroblasts are also known to express certain nAChR subtypes (24). We observed that nAChRα1 expression was significantly higher in the kidneys of uPAR-deficient mice that develop worse scarring during UUO (supplemental Fig. S1*a*).

Evidence that nAChRα1 might function as an alternative uPA receptor was suggested by our microarray data that compared $uPAR^{-/-}$ and $uPAR^{+/+}$ renal fibroblasts. The nAChRα1 was the only one of the 12 receptor candidates identified by Liang *et al.* (17) that was significantly up-regulated on the $uPAR^{-/-}$ fibroblasts ($n = 5$, $p < 0.01$ by analysis of variance (ANOVA), >2-fold change) (supplemental Fig. S1*b*). Based on the assumption that the receptor may be up-regulated in damaged kidneys in the absence of uPAR and contribute to the development of more severe fibrosis, this study was designed to determine if a ligand-receptor relationship exists between uPA and nAChRα1 and to investigate its functional role in fibroblast growth and renal fibrosis. *In vivo* functional knockdown of the nAChRα1 was shown to significantly attenuate fibrosis after ureteral obstruction, an effect that was uPA-dependent. *In vitro* studies provided additional evidence that nAChRα1 was an uPA signaling receptor for fibroblasts, activating a complex of signaling proteins by tyrosine phosphorylation and calcium influx to stimulate proliferation and enhance contractility.

EXPERIMENTAL PROCEDURES

Antibodies and Reagents—Antibodies used in this study and their sources were as follows: rabbit anti-mouse uPA, Molecular Innovations Inc. (Novi, MI); antibodies to nAChRα1, -β1, or -γ and FGF-2, Santa Cruz Biotechnology, Inc. (Santa Cruz, CA); antibodies to uPAR1, phosphotyrosine, and E-cadherin (R&D Systems, Minneapolis, MN); rat monoclonal antibody to F4/80, Serotec Ltd. (Oxford, UK); EPO™ horseradish peroxidase-conjugated monoclonal antibodies to vimentin, αSMA, or PCNA and rat monoclonal antibody to Ki-67 (TEC-3), Dako Corp. (Carpinteria, CA); rabbit monoclonal antibody to Ki-67 (SP6), Novus Biologicals Inc. (Littleton, CO); rabbit antibody to receptor-conjugated choline glutaric acid (receptor-bound acetylcholine), Abcam Inc. (Cambridge, MA); fluorescein isothiocyanate-conjugated antibody to β-actin, Sigma; and rat anti-bromodeoxyuridine (BrdUrd) monoclonal antibody (Harlan SERA-LAB, Loughborough, UK). Protein reagents used in the *in vitro* intervention studies were as follows: active mouse urokinase (uPA) and amino-terminal fragment of mouse uPA (ATF), Molecular Innovations, Inc.; α-bungarotoxin (αBTx), D-tubocurarine (*d*-TC), and neonicotine (neoN), Sigma. High protein rat tail collagen, type 1 (12.29 mg/ml), used in forming a three-dimensional gel, was purchased from BD Biosciences.

siRNA-expressing Constructs—Several siRNA hairpin oligonucleotides to the target nAChRα1 mRNA sequence (NM-007389) were designed and synthesized using a strategy described previously (25) (supplemental Fig. S2*a*). A scrambled RNA hairpin oligonucleotide was produced as a control. The hairpin inserts were cloned into the Promega *psisTRIKE*™ vector (Promega Corp.) according to the manufacturer's instruction. Following transformation and amplification in *Escherichia coli* bacteria, plasmid DNA was isolated, digested with PstI, and confirmed by DNA sequencing (supplemental Fig. S2*b*). The silencing efficacy of these constructs was tested in renal fibroblast cultures (supplemental Fig. S2, *c* and *d*). The vector with the highest silencing effect against nAChRα1, which targets mouse nAChRα1 sequence at 1213–1238, was named *psir2*. The vector expressing the scrambled RNA sequence (GGCAUAAGAUUUAGCGGCAAGCAAU) was designated as *pscr*.

Animals and in Vivo RNA Interference Studies—All animal studies were approved by the Institutional Animal Care and Use Committee of the Seattle Children's Research Institute. All mice were on a C57BL/6 background. Wild-type (WT) mice were purchased from the Jackson Laboratory and underwent UUO surgery and cDNA intervention experiments at 12 weeks of age, as reported previously (26). To functionally knock down nAChRα1 expression, the *psir2* naked plasmid DNA was administered via tail veins ($n = 10$) using a hydrodynamic protocol as described previously (27, 28). Controls were injected with *pscr* plasmid DNA. Following rapid tail vein injection of 100 μg of DNA (*psir2* or *pscr*) in 1 ml of normal saline, UUO surgery was performed in the left kidney. Kidneys and other tissues were harvested 7 days later. Additional mice were injected with *pEGFP* (a plasmid cDNA encoding enhanced green fluorescence protein obtained from Invitrogen using the same procedure. In order to delineate the functional relation-

ship between nAChRα1 and uPA, urokinase-deficient *Plau*$^{-/-}$ mice (29) were obtained from the Jackson Laboratories (Bar Harbor, ME) and used in another set of RNA interference experiments, as described above for the WT mice.

Cell Culture and Stable Transfection—Primary renal fibroblast cultures were used as an *in vitro* model to further identify, characterize, and delineate this potential ligand-receptor relationship and to investigate its functional effects on renal fibroblasts. Wild-type and *uPAR*$^{-/-}$ mouse renal fibroblast primary cultures were established and characterized as previously described (16). Cells were routinely cultured at 37 °C with 5% CO_2 in DMEM/F-12 (1:1) supplemented with 5% (v/v) fetal calf serum (pH 7.35–7.45) and were passed after treatment with 0.05% trypsin, 0.53 mM EDTA digestion buffer (Mediatech Inc., Manassas, VA). The *psir2* and *pscr* cDNAs were transfected into the *uPAR*$^{-/-}$ cells, using siPORT™ *XP-1* transfection agent (Ambion Inc., Austin, TX) according to the manufacturer's instructions. Neomycin-resistant cell clones were selected and amplified. The cellular nAChRα1 silencing efficiency was confirmed at the mRNA and protein levels (supplemental Fig. S3). All *in vitro* experiments were performed, and results were compared with cells at 8–10 passages.

Northern Blotting and Quantitative Real Time PCR—Total RNA was isolated from cells or kidneys using TRIzol™ reagent (Invitrogen) according to the manufacturer's protocol. Northern blot analysis for αSMA (26) and uPAR (30) and TaqMan real time reverse transcription-PCR for nAChRα1 were performed as described previously (24, 26).

Immunohistochemical (IHC) and Immunofluorescent Stains and Morphometric Analyses—The nAChRα1 and phosphotyrosine were immunolabeled in cultured renal fibroblasts using a standard ABC kit protocol (Vector Laboratories) (30, 31). Paraffin-embedded kidney sections were stained with primary antibodies to nAChRα1, receptor-conjugated choline glutaric acid (receptor-bound acetylcholine), αSMA, Ki-67, and FGF-2. For IHC double staining, anti-αSMA antibody was directly labeled with horseradish peroxidase (developed with 3,3′-diaminobenzidine plus nickel, resulting in a black color), and nAChRα1 or Ki-67 was indirectly labeled with alkaline phosphatase-conjugated secondary antibodies (developed with Fast Red, resulting in a red color) (26). For immunofluorescent double stains, uPA and nAChRα1 were identified with fluorescein isothiocyanate (green) and tetramethylrhodamine (red) fluorescence, respectively. Images were captured with a SPOT camera. For αSMA and receptor-bound acetylcholine, positive stain was quantified using Image-Pro Plus software. For nAChRα1, the staining in glomeruli, tubules, and the interstitium was separately quantified using the Image-Pro Plus software (for glomeruli) or a previously published point-counting method (for tubular or interstitial areas) (30). The results were expressed as positive percentage of area of interest (glomerular, tubular, or interstitial areas).

Total Collagen Assay—Total renal collagen was measured biochemically, as previously described (26). In brief, an accurately weighed portion of the kidney was homogenized in distilled water, hydrolyzed in 10 N HCl, and incubated at 110 °C for 18 h. The hydrolysate was dried by speed-vacuum centrifugation and redissolved in buffer (25 g of citric acid, 6 ml of glacial acetic acid, 60 g of sodium acetate, and 17 g of sodium hydroxide in 500 ml (pH 6.0)). Total hydroxyproline in the hydrolysate was determined according to the chemical method of Kivirikko *et al.* (32). Total collagen in the tissue was calculated on the assumption that collagen contains 12.7% hydroxyproline by weight. Final results were expressed as μg/mg kidney wet weight.

Western Immunoblotting and Co-immunoprecipitation—Immunoblotting (IB) and co-immunoprecipitation (IP/IB) experiments were performed following standard protocols (33).

Flow Cytometry Studies—Fibroblast nAChRα1 protein expression was evaluated using a standard flow cytometric approach. Renal fibroblasts were cultured in medium with or without uPA (2.4×10^{-8} M, a dose selected based on its binding K_d and our previous dose-response studies) (16). At the end of the experiment (from 24 to 72 h), cells were harvested and subsequently incubated with ab1 specific for nAChRα1 and fluorescein isothiocyanate-conjugated ab2. Following stringent washes, cells were counted, and fluorescence intensities were evaluated using a flow cytometry (FACSCalibur; BD Biosciences).

Fibroblast Proliferation Assays—Fibroblast proliferation was evaluated using the CellTiter 96 Aqueous One Solution cell proliferation kit (Promega) according to the manufacturer's instructions (16). Since *uPAR*$^{+/+}$ fibroblasts did not survive for 72 h in serum-free culture conditions, uPA (2.4×10^{-8} M)-stimulated cell proliferation experiments were performed in DMEM/F-12 medium with 0.1% fetal calf serum. Similar stimulating experiments using *uPAR*$^{-/-}$ fibroblasts were performed under serum-free conditions. For each genotype, fibroblast proliferation was measured over several time periods in the presence or absence of uPA stimulation, comparing the responses of nAChRα1-expressing and -silenced fibroblasts. Each experiment was typically performed with $n = 12$ separate wells of fibroblasts in 96-well plates. Control experiments were performed with neoN and αBTx serving as an nAChRα1 agonist or antagonist, respectively. In additional experiments, nuclear mitotic activity was assessed by flow cytometric analysis of BrdUrd incorporation (34). BrdUrd was added to the culture medium (final concentration 400 μg/ml) and incubated for 2 h prior to the experimental end point. Cells were then harvested, and their DNA was denatured with 2 N HCl at 37 °C for 30 min. BrdUrd was revealed with a rat anti-BrdUrd monoclonal antibody (1:10). Secondary antibody was goat anti-rat coupled to fluorescein isothiocyanate (Southern Biotechnology Associates, Birmingham, AL). Cell fluorescence intensity was evaluated using a flow cytometry (FACSCalibur; BD Biosciences), with the results expressed as a percentage of BrdUrd-positive cells (BrdUrd incorporation rate).

Collagen Gel Contraction Assay—The ability of the uPA-nAChRα1 interactions to modulate fibroblast-mediated collagen gel contraction was determined using the three-dimensional collagen gel slow contraction assay, as previously described (35). Briefly, fibroblasts were incubated in DMEM containing type I collagen (0.75 mg/ml) with or without uPA (2.4×10^{-8} M) to form a three-dimensional collagen lattice. The gels released from the plate wells were incubated in DMEM

plus 1% fetal calf serum for 4 days. The gel area was measured at 0, 48, and 96 h.

Urokinase and Nicotine Binding Assays—In an effort to determine if nAChRα1 mediates uPA binding to $uPAR^{-/-}$ fibroblasts, urokinase and nicotine competition binding studies were performed. Urokinase binding assays were carried out using two strategies. In the first, serial concentrations of the labeled uPA and a fixed concentration of the competitive inhibitor α-BTx were simultaneously added to the cells to measure binding competition using a classical assay described by Mazzieri *et al.* (36). The uPA (American Diagnostic, Hauppauge, NY) was labeled using the DSB-X Biotin Protein Labeling Kit (Invitrogen) and streptavidin-^{35}S (GE Healthcare) according to the manufacturers' instructions. In order to determine binding specificity, experiments were performed with or without a 100-fold excess of unlabeled uPA, in the presence of the nAChRα1 competitive antagonist α-BTx (0.1 μM) or in the absence of receptor nAChRα1 (receptor-silenced cells). After stringent washes, emitted β-activities were counted. In the second binding study strategy, the nAChRα1 expressed by $uPAR^{-/-}$ fibroblasts was preblocked with 0.1 μM α-BTx or a gradient concentration of *d*-TC for 30 min before the addition of biotinylated uPA (2.4×10^{-8} M). A previously published co-IP method (37) was used to pull down the nAChRα1-bound uPA with an antibody specific for nAChRα1. The immunoprecipitated proteins were then run in an SDS gel and transferred to a membrane, and the biotinylated uPA was probed with ImmunoPure streptavidin-rhodamine (Pierce). Blots were scanned, and the fluorescence intensity was analyzed using a Typhoon 9410 variable mode imager (Amersham Biosciences). Nicotine binding assays were performed with serial concentrations (from 1.8 to 600 nM) of ^{3}H-labeled nicotine (PerkinElmer Life Sciences) at room temperature for 45 min. Competition binding was carried out in the presence of pre-exposed uPA (10^{-7} M) or *d*-TC (15 μM) (added 30 min earlier than [^{3}H]nicotine). All binding assay data were analyzed and graphed with GraphPad Prism 4 software.

uPA/nAChRα1-induced Phosphorylation Studies—In an effort to determine if uPA binding to nAChRα1 activates intracellular signal transduction by tyrosine phosphorylation, 90% confluent $uPAR^{-/-}$ fibrobroblast cultures were rendered quiescent in serum-free medium (SFM) overnight and then stimulated with 2.4×10^{-8} M uPA in SFM for a period of time from 0 to 30 min. Two strategies were employed to determine if the nAChRα1 initiates uPA signaling: 1) by comparing signal activation in nAChRα1-silenced $uPAR^{-/-}$ fibroblasts *versus* nAChRα1-overexpressing $uPAR^{-/-}$ fibroblasts and 2) by identifying the activation (phosphorylation) of nAChRα1 *per se* with the IP/IB method. Cells grown on glass coverslips were fixed in 4% paraformaldehyde and stained with a phosphotyrosine-specific antibody using the ABC kit. Proteins extracted with 5% SDS buffer were used in IB analyses for phosphotyrosine and in IP/IB studies for phosphorylated receptor nAChRα1. Components of the signaling pathway were further identified by phosphoproteomic mass spectrometry experiments.

Phosphoproteomic Mass Spectrometry—Phosphoproteins expressed by $uPAR^{-/-}$ fibroblasts before and after uPA (2.4×10^{-8} M) stimulation were isolated and enriched by immunoprecipitation using an antibody specific for phosphorylated tyrosine residues. The pull-down proteins were separated by one-dimensional gel electrophoresis under a nonreduced condition. The bands stained with SimpleBlue™ SafeStain (Invitrogen) were excised from the gel, and the tryptic peptide fingerprint was analyzed by matrix-assisted laser desorption ionization time-of-flight mass spectrometry.

Ca^{2+} Mobilization Assays—Fibroblasts were grown in SFM for 36 h and loaded with the $[Ca^{2+}]_i$-sensitive probe fura-2 AM at 37 °C for 30 min. The change in fluorescence intensity before and after uPA (2.4×10^{-8} M) stimulation was measured using either the microfluorimetric technique of the TILLVISION program (Till Photonics GmbH Inc., Gräfelfing, Germany) for cells grown on glass coverslips or a spectrofluorimeter (Photon Technology International, Birmingham, NJ) for cell suspensions, as previously described (38). Intracellular calcium was monitored as 500 nm fluorescence emission following 340/380 nm excitations.

Patch Clamp Studies—Patch clamp experiments were performed in the tight seal on-cell configuration at 24 ± 2 °C, as described by Akk and Steinbach (39). Fibroblasts grown on glass coverslips were transferred to the recording chamber and kept in a standard modified bath solution containing 137 mM $NaCl_2$, 2.4 mM $CaCl_2$, 2.7 mM KCl, 0.5 mM $MgCl_2$, 6.6 mM Na_2HPO_4, 1.5 mM KH_2PO_4, pH 7.3. Base-line patch pipette resistances were between 2 and 4 megaohms when the pipette was filled with a solution of 142 mM KCl, 1.8 mM $CaCl_2$, 1.7 mM $MgCl_2$, 5.4 mM $NaCl_2$, 10 mM Hepes, pH 7.4. Following the addition of uPA (2.4×10^{-8} M) to the bath solution, high resolution current recordings were acquired using a computer-based patch-clamp amplifier system (EPC-9, HEKA, Lambrecht, Germany). Additional experiments were performed after preblocking nAChRα1 with *d*-TC (1.5×10^{-5} M in the bath solution) for 10 min prior to uPA stimulation. The membrane potential was held at −50 mV. Results were expressed as current amplitude changes with time or current-voltage (*I*-V) curves.

Microarray Gene Expression Experiments—Using previously published methods (40), microarray experiments were conducted using the Affymetrix mouse 430 2.0 chip (45,102 probe sets) in four experimental groups: *pscr*, $uPAR^{-/-}$ fibroblasts with or without uPA (2.4×10^{-8} M) and *psir*, $uPAR^{-/-}$ fibroblasts with or without uPA (2.4×10^{-8} M). All groups were cultured for 48 h in DMEM/F-12 medium containing 0.5% fetal calf serum. Each experiment compared five sets of $uPAR^{-/-}$ fibroblast cultures per group, unstimulated *versus* uPA-stimulated; -fold change >2.5, $p < 0.0001$ by ANOVA considered statistically significant.

Statistical Analyses—Data were analyzed using Student's *t* test (parametric data) or Mann-Whitney *U* test (nonparametric data), and the null hypothesis was rejected at a *p* value less than 0.05 unless specified elsewhere (*e.g.* microarray data analyses). Values are presented as mean ± 1 S.D. unless stated otherwise.

RESULTS

Renal Expression of nAChRα1 and Acetylcholine during Fibrogenesis—In wild-type mouse kidneys, nAChRα1 protein is expressed in all compartments of the cortex, including glomeruli, tubules, and the interstitium, but absent in the medulla. Glomerular and tubular nAChRα1 expression rapidly declined during UUO (>6-fold reduction by day 7, evaluated by IHC). In contrast, expression by interstitial cells was strongly up-regulated, especially within fibrotic areas of the renal cortex (Fig. 1*a*). By double immunostaining, the interstitial nAChRα1 protein co-localized to αSMA^+ myofibroblasts in the obstructed kidneys (Fig. 1*b*). However, given the striking reduction in glomerular and tubular expression, total kidney nAChRα1 protein levels were significantly lower on day 7 UUO compared with sham-operated mice (Fig. 1*c*).

In preliminary studies using a green fluorescent protein transgene, the tail vein hydrodynamic DNA delivery system was shown to achieve significant gene expression within tubulointerstitial and glomerular cells in obstructed kidneys (Fig. 2*a*). Using this delivery system, nAChRα1 protein expression was significantly reduced by 70% (day 7 UUO) with the siRNA-expressing plasmid DNA (Fig. 2*b*).

Acetylcholine (ACh) is the only currently known endogenous ligand for nAChRα1, and very little immunochemically detectable receptor-bound ACh is present in normal kidneys (Fig. 2*c*). The bound ACh ligand substantially increased in the obstructed kidneys 7 days after UUO ($n = 6$, $p < 0.05$, UUO *versus* sham). The bound ACh was seen exclusively on glomerular and tubular cells. The glomerular and tubular receptor-bound ACh was significantly reduced in the nAChRα1-knockdown mice (2.6-fold less, $n = 6$, $p < 0.05$, *psir2 versus pscr*, 7 days after UUO). No bound ACh was found in tubulointerstitium, suggesting that ACh is not the primary functional ligand for the increased interstitial fibroblastic nAChRα1 receptor during fibrogenesis and that an alternative ligand may present.

The nAChRα1 Is Functionally Important to Fibrotic Responses to Renal Injury—After a 70% knockdown of nAChRα1 in the wild-type mice, there was a 2.8-fold reduction in the number of the αSMA^+ interstitial myofibroblasts compared with the *pscr*-treated mice ($p < 0.05$, *psir2 versus pscr*, $n = 8$, 7 days after UUO) (Fig. 3*a*). This effect was coupled with suppressed FGF-2 (fibroblast growth factor-2, also called basic fibroblast growth factor) protein levels in the nAChRα1-silenced mice (98% inhibition, $n = 6$, $p < 0.05$, *psir2 versus pscr*) (Fig. 3*b*). The reduced interstitial myofibroblast recruitment was probably due in part to an inhibition of the cell proliferation response (PCNA and Ki-67 levels reduced by 93 and 60% in Western analyses, respectively, *psir2 versus pscr*, $n = 6$, both $p < 0.05$, 7 days after UUO); IHC stain/double stain determined that the Ki-67^+ proliferating cells in the obstructed kidneys were almost exclusively interstitial myofibroblasts (Fig. 3*b*).

The decrease in interstitial myofibroblasts was associated with less severe tubular cell dedifferentiation, as reflected by higher E-cadherin levels in the *psir2*-treated mice ($p < 0.05$, *psir2 versus pscr*, $n = 4$, 7 days after UUO) (Fig. 3*c*), probably as a consequence of reduced myofibroblast numbers and the ensuing fibrosis attenuation. The degree of fibrosis was significantly reduced by 24%, measured as total kidney collagen ($p < 0.05$, *psir2 versus pscr*, $n = 8$, 7 days after UUO) (Fig. 3*c*).

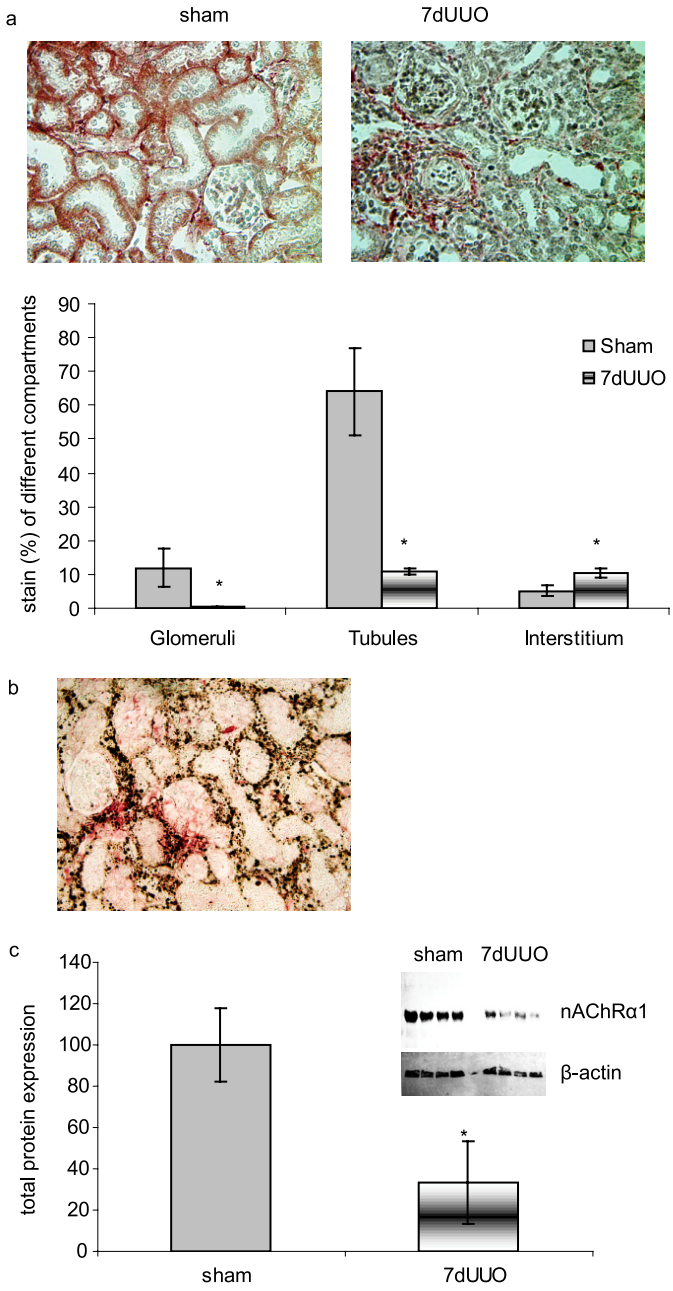

FIGURE 1. **Renal expression of nAChRα1.** *a*, nAChRα1 IHC staining detects a strong expression in glomeruli and cortical tubules in a normal mouse kidney. Seven days after UUO, expression localizes to interstitial cells, whereas glomerular and tubular expression has largely disappeared. Using either the Image-pro program (for glomeruli) or a point-counting method (for tubular or interstitial areas), compartment-specific nAChRα1 expression was quantified, and results are expressed as positive percentage of area of interest. *b*, IHC double staining co-localizes αSMA^+ (*brown*) and nAChRα1 (*red*) staining to a subpopulation of interstitial cells in an obstructed kidney 7 days after UUO. *c*, nAChRα1 Western blot analysis shows significantly reduced expression after UUO. The β-actin bands were used to correct for protein loading. The *histogram* represents the relative band densities analyzed with the NIH Image program ($n = 8$). *, $p < 0.05$, sham *versus* 7-day UUO (*7dUUO*). Original magnification was ×400.

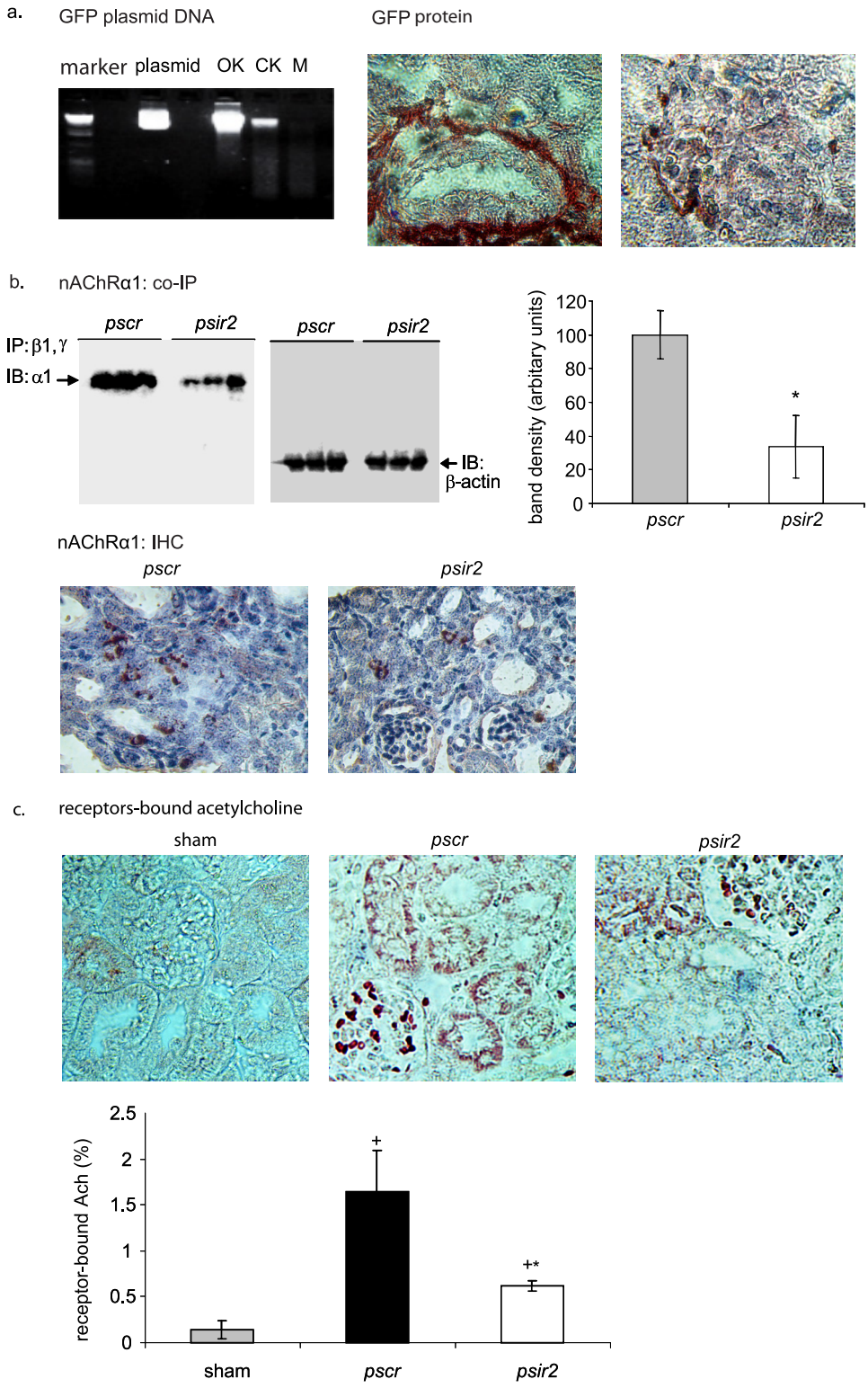

FIGURE 2. **Targeted knockdown of kidney nAChRα1 and the expression of receptor-bound ACh.** The hydrodynamic high pressure intravenous approach effectively delivered plasmid DNA to both the obstructed (*OK*) and the contralateral kidney (*CK*). *a*, the *pEGFP* plasmid DNA encoding enhanced green fluorescence protein was detected in mouse whole kidney but not in muscle tissue (*M*) by agarose gel electrophoresis. Pure plasmid DNA served as molecular size control. On the *right*, green fluorescent protein immunohistochemical staining illustrates green fluorescent protein expression in both tubulointerstitial and glomerular cells of the obstructed kidneys 7 days after UUO. *b*, co-immunoprecipitation studies showed significantly less renal nAChRα1 protein in *psir2*-treated mice compared with the *pscr* mice (*, $p < 0.05$, $n = 6$). *IP*, antibodies used for immunoprecipitation; *IB*, antibody used for immunoblotting. The *graph* shows the mean immunoblot band densities ± 1 S.D., corrected for protein loading using β-actin protein band densities. Kidney nAChRα1 IHC staining illustrates lower levels in the *psir2* mice. *c*, IHC staining using an antibody that detects receptor-bound but not free acetylcholine (*Ach*) was negative in the normal sham kidney; significant glomerular and tubular (but not interstitial) staining was observed in obstructed kidneys. The *histogram* illustrating the results of computer-assisted image analysis of the receptor-bound ACh^+ area shows a significant 70% reduction in the nAChRα1-silenced group 7 days after UUO. *, $p < 0.05$, *psir2 versus pscr*, 7-day UUO, $n = 8$; +, $p < 0.05$, sham *versus* 7-day UUO, $n = 8$/group. Original magnification was ×600 (*a*) or ×400 (*b* and *c*), counterstained with hemotoxylin.

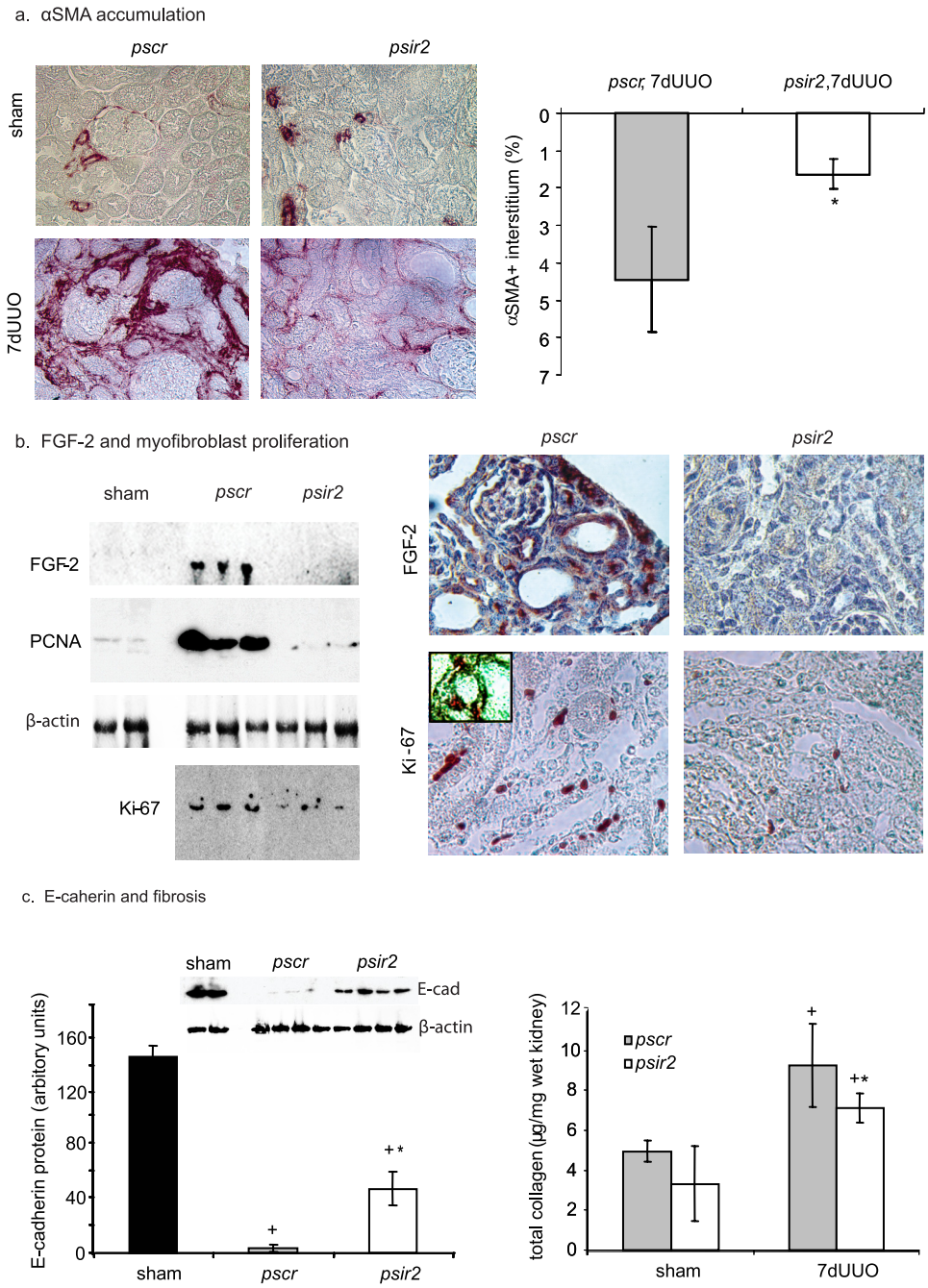

FIGURE 3. **nAChRα1 silencing reduces myofibroblast proliferation and renal fibrosis.** *a*, IHC photomicrographs illustrate differences in the number of kidney αSMA$^+$ myofibroblasts in mice treated with the nAChRα1 silencing (*psir2*) and scrambled (*pscr*) siRNA. The *graph* summarizes the results of computer-assisted image analysis of the αSMA$^+$ interstitial area, showing a significant 74% reduction in the nAChRα1-silenced group 7 days after UUO. *b*, kidney protein levels for the cell cycle proteins Ki-67, PCNA, and mitogenic fibroblast growth factor (*FGF-2*) are reduced in the nAChRα1-knockdown kidneys (*psir2*) compared with the scramble controls (*pscr*), as shown in the Western blot analyses (FGF-2 and PCNA) or by first concentrating the sample by pulling down (immunoprecipitation with the rabbit monoclonal anti-Ki67 antibody) and then probing (immunoblot with the rat monoclonal antibody) for Ki-67. All *p* values were <0.05, *psir2 versus pscr*, $n = 6$, 7-day UUO. By IHC, FGF-2 was detected in both tubules and interstitial cells in the obstructed kidneys of the control group. Reduced numbers of proliferating kidney interstitial cells in the nAChRα1 siRNA-treated mice after UUO are illustrated by IHC stain for Ki-67. The *inset photograph* illustrates double staining for Ki-67 and αSMA (αSMA in *black*, Ki-67 in *red*), indicating that the majority of Ki-67$^+$ cells are αSMA$^+$ fibroblasts. *c*, kidney E-cadherin Western blot illustrates significantly higher levels in the nAChRα1-knockdown mice after ureteral ligation, indicative of less tubular damage. The lower β-actin stained bands were used to correct for protein loading. The *histogram* represents the relative band densities, analyzed with the NIH Image program. Total kidney collagen levels (measured using the hydroxyproline assay) were significantly lower in the kidneys of mice treated with the AChRα1-siRNA construct. *, $p < 0.05$, *psir2 versus pscr*, 7-day UUO, $n = 8$; +, $p < 0.05$, sham *versus* 7-day UUO (*7dUUO*), $n = 8$/group. Original magnification was ×400 (*a* and *b*).

Fibroblastic nAChRα1 Expression and nAChRα1-promoted Myofibroblasts Are uPA-dependent—To investigate the role of uPA as a potential fibroblast nAChRα1 ligand, the UUO-induced renal myofibroblastic response on day 7 was compared between WT C57BL/6 and *uPA*$^{-/-}$ C57BL/6 mice after administration of *pscr* or *psir2*. Similar to the observation in wild-type mice, nAChRα1 protein was mainly expressed by tubules in normal kidneys; levels significantly declined 8-fold in response to ureteral obstruction and further decreased in the *psir2*-treated mice compared with the *pscr*-treated mice on day 7 after UUO (Fig. 4*a*). However, unlike the wild-type mice, the expanding interstitial cell population expressed very little nAChRα1 in the absence of uPA. The αSMA expression levels, as measured by Northern blot analyses, were similar in the *pscr*- and *psir2*-treated uPA-deficient mice at 7 days after UUO (Fig. 4*b*). This was confirmed by Western blot analyses (data not shown).

The *in vivo* finding suggesting that uPA may induce renal fibroblastic nAChRα1 expression and promote myofibroblast recruitment was further investigated *in vitro*. Following a 24-h incubation in SFM with or without uPA (2.4×10^{-8} M), flow cytometric analyses demonstrated a significantly higher percentage (35% increase) of nAChRα1-positive renal fibroblasts in the uPA-stimulated group compared with the unstimulated control group ($p < 0.05$, three independent experiments) (Fig. 5*a*). Northern blot analyses were performed to investigate the effects of uPA-nAChRα1/uPAR interactions on fibroblast αSMA expression, a cytoskeleton protein marker for "activated" fibroblasts or myofibroblast phenotypic transformation (41, 42) (Fig. 5*b*). The full-length active uPA, but not the ATF, which lacks the catalytic domain but still binds to uPAR, upregulated αSMA gene expression in wild-type fibroblasts that expressed both receptors. The absence of both receptors completely nullified the

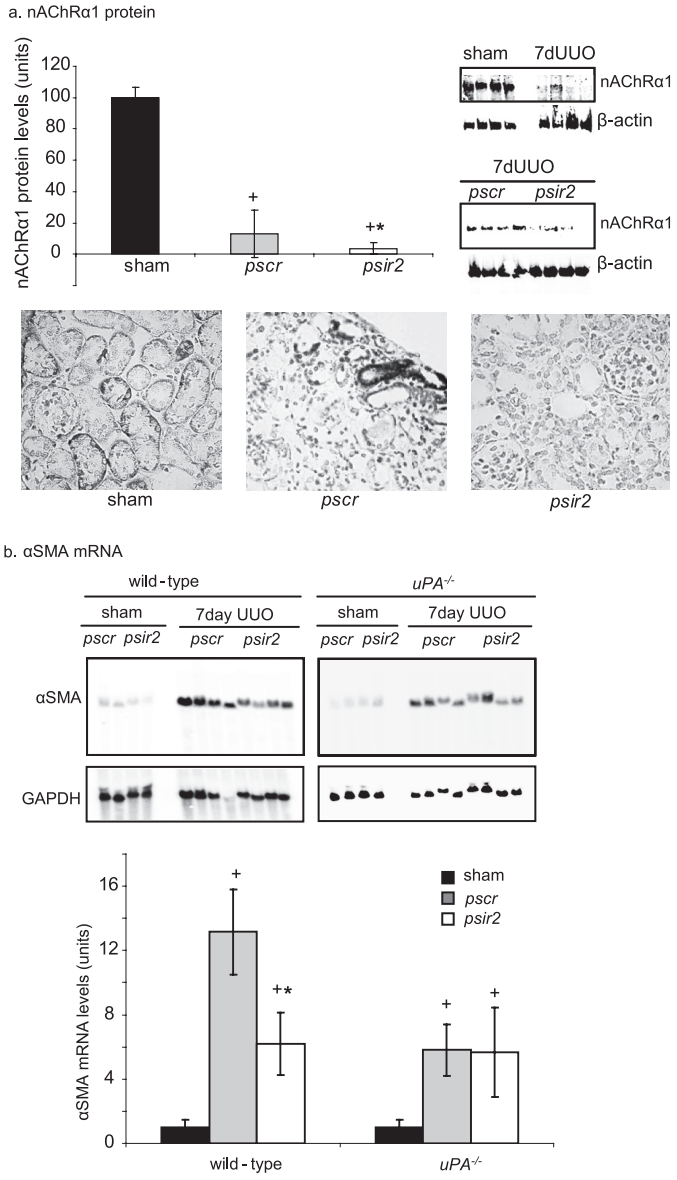

FIGURE 4. **The nAChRα1-dependent myofibroblast recruitment requires uPA.** *a*, renal nAChRα1 Western blot analysis illustrates a significant reduction in total nAChRα1 protein in the $uPA^{-/-}$ mice after UUO, as was observed in the wild-type mice shown in Fig. 1. The *histogram* represents mean band densities. +, $p < 0.05$, sham *versus* 7-day UUO (*7dUUO*), $n = 4$/group; *, $p < 0.05$, *psir2 versus pscr*, 7-day UUO, $n = 4$. The nAChRα1 IHC photomicrographs illustrate that the nAChRα1 protein was absent in the interstitium of both normal and obstructed $uPA^{-/-}$ kidneys. *b*, kidney αSMA. Northern blot analysis illustrates a significant 2-fold reduction in αSMA mRNA due to nAChRα1-silencing seen in the uPA-sufficient mice 7 days after UUO but not in the $uPA^{-/-}$ mice ($n = 8$). The *histogram* represents semiquantitative results (mean ± S.D.) of Northern blot analysis using the NIH Image analysis program. The lower glyceraldehyde-3-phosphate dehydrogenase (*GAPDH*) mRNA bands were used to correct for RNA loading.

uPA effects on αSMA induction. Fibroblasts bearing uPAR or nAChRα1 alone showed significantly lower αSMA mRNA levels in response to either the full-length uPA or ATF, suggesting that uPA may require concurrent interaction with both receptors to transform fibroblasts.

The uPA-nAChRα1 Interaction Regulates Fibroblastic Growth and Contractility in Vitro—We previously reported (16) that renal fibroblasts produce uPA and that uPA stimulates proliferation both in $uPAR^{+/+}$ and $uPAR^{-/-}$ fibroblasts. Given our *in vivo* findings, which suggest that nAChRα1-uPA signaling may regulate the number of interstitial myofibroblasts that appear in response to chronic kidney injury, the ability of this interaction to stimulate renal fibroblast proliferation was investigated *in vitro* by comparing nAChRα1-expressing and -silenced fibroblasts. Although the addition of uPA in culture media moderately stimulated renal fibroblast proliferation regardless of their uPAR status, the absence of nAChRα1 completely abrogated the growth-promoting effect of the exogenous uPA ($n = 10$, $p < 0.05$, two independent studies) (Fig. 6*a*). Control experiments showed that uPA stimulated $uPAR^{-/-}$ fibroblast proliferation to the same extent as 1 nM neoN. Both were blocked by the addition of 0.1 μM αBTx ($n = 10$, all $p < 0.05$). In 48-h $uPAR^{-/-}$ fibroblast cultures, the uPA-stimulated BrdUrd incorporation rates were significantly lower in the absence of the nAChRα1 receptor (27.9 ± 2.2% *versus* 18.9 ± 4.8%, $p < 0.05$, *pscr versus psir2*, three independent experiments).

When adherent cells are partially detached, they morphologically become round due to spontaneous contraction. This change in phenotype is the basis of the *in vitro* single-cell contraction assay reported previously (43). During our routine passing of renal fibroblast cultures, we noticed that the nAChRα1-silenced $uPAR^{-/-}$ fibroblasts took significantly longer to become round in shape when compared with the nAChRα1-overexpressing $uPAR^{-/-}$ fibroblasts (30 ± 5 min *versus* 15 ± 3 min, $p < 0.05$, three independent experiments), suggesting differences in their adherence and/or contraction (Fig. 6*b*). Given this finding and the known importance of the contractile properties of wound-associated fibroblasts during scarring (44), the effect of nAChRα1 on matrix contraction was addressed more directly using a gel contraction assay. Gel contraction was greatest in the nAChRα1-overexpressing $uPAR^{-/-}$ cells (*pscr*-transfected), weakest in the nAChRα1-silenced $uPAR^{-/-}$ cells (*psir2*-transfected), and intermediate in the wild-type cells ($n = 4$, $p < 0.05$, both 48 and 96 h) (Fig. 6*b*). These data suggest that the receptor nAChRα1 is involved in triggering the mitogenic and motogenic functions of fibroblasts.

Urokinase Is a Specific Ligand for Renal nAChRα1 Receptor both in Vivo and in Vitro—In the next series of experiments, we investigated whether uPA can directly bind to the fibroblast nAChRα1 receptor. The uPA protein co-localized with the nicotinic receptor nAChRα1 in obstructed kidneys (Fig. 7*a*). The nAChRα1 receptor (in both interstitium and tubules) was totally overlapped with the uPA, but not all uPA protein was physically associated with the cellular nAChRα1. Co-IP studies were performed to further analyze the possibility of a specific uPA-nAChRα1 ligand-receptor relationship using renal proteins isolated from the wild-type and uPA-null mice. These data showed that uPA protein can bind to the nicotinic receptor nAChRα1 in both normal and fibrotic kidneys (Fig. 7*a*). The amount of uPA protein that was pulled down was highly correlated with each receptor ($r_{(uPA/nAChR\alpha1)} = 0.92$; $r_{(uPA/uPAR)} = 0.99$; $n = 6$, both $p < 0.05$). The fact that uPA was required in order to co-immunoprecipitate nAChRα1 and uPAR suggests that uPA either bound to each receptor via distinct sites or induced a conformational change that enabled direct binding

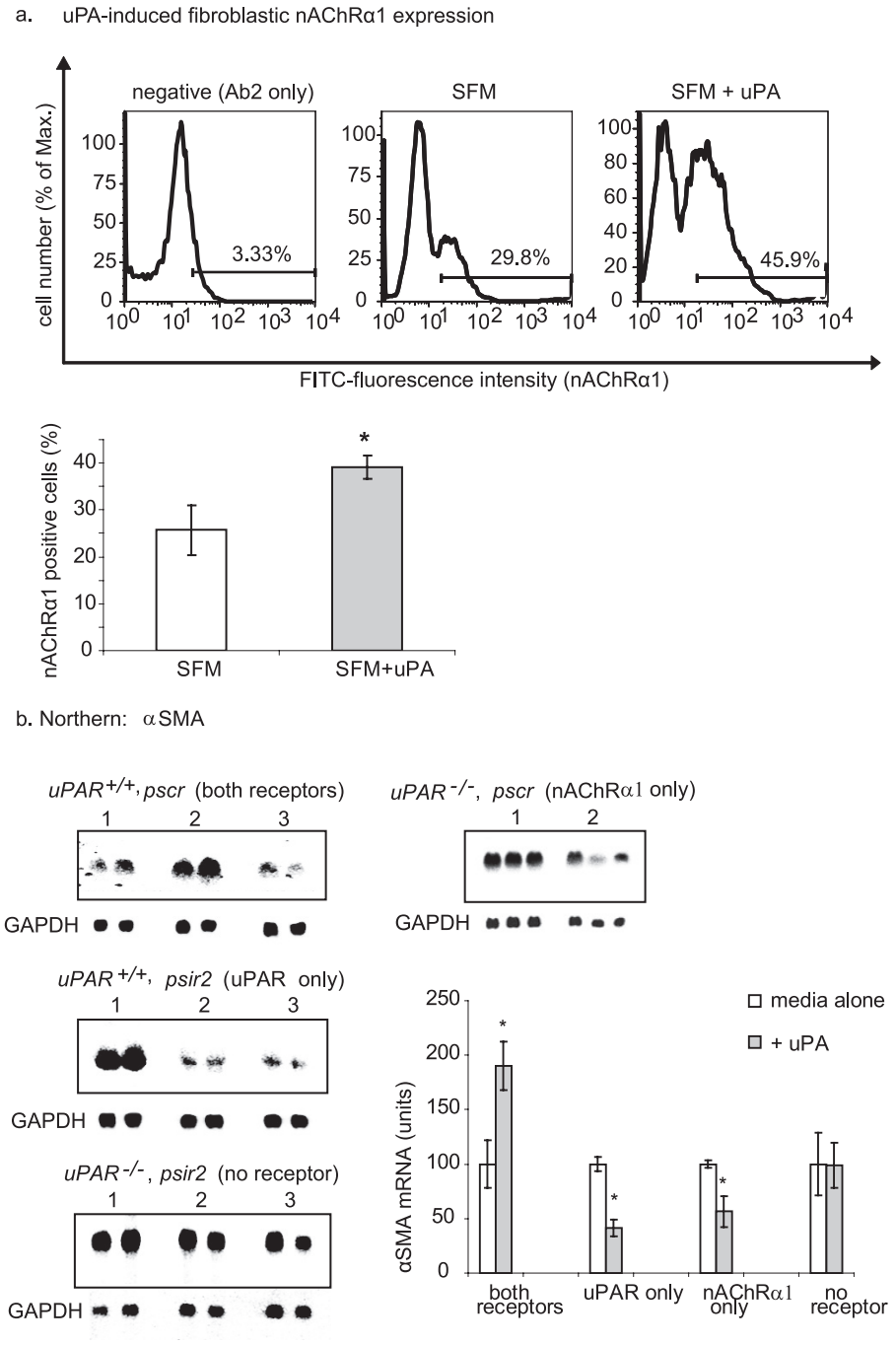

FIGURE 5. **The uPA induces fibroblastic nAChRα1 and αSMA expressions.** *a*, flow cytometric analyses illustrates that fibroblastic nAChRα1 expression was significantly up-regulated by incubation with uPA (2.4×10^{-8} M) for 24 h in serum-free medium (*SFM*). The *histogram* summarizes the results of three independent experiments ($n = 3$; *, $p < 0.05$, SFM + uPA *versus* SFM alone). Cells stained with Ab2 alone were used as a negative control. *b*, Northern blot analysis illustrating receptor-dependent effects of uPA treatment for 48 h on fibroblast αSMA gene expression (representative blot from two independent experiments). The uPA promotes αSMA gene expression when both receptors are present. However, uPA down-regulates αSMA gene expression when either receptor is expressed alone. *Lanes 1*, media only; *lane 2*, uPA (2.4×10^{-8} M); *lane 3*, uPA ATF (1×10^{-8} M). *Blots below* each αSMA Northern are glyceraldehyde-3-phosphate dehydrogenase (*GAPDH*) bands to demonstrate RNA loading equality. The *histogram* represents the relative band densities analyzed with the NIH Image program ($n = 4$). *, $p < 0.05$, uPA$^+$ *versus* media alone.

between the two uPA receptors. A specific interaction between uPA and cell surface nAChRα1 was further demonstrated by *in vitro* cell binding assays using renal fibroblasts (Fig. 7*b*) that expressed different levels of the receptor nAChRα1. ^{35}S-Labeled uPA bound to the uPAR-null, endogenously nAChRα1-overexpressing renal fibroblasts with $K_d = 1.6 \times 10^{-8}$ M. Binding was competitively inhibited in the presence of a 100-fold excess of non-labeled uPA and by the nAChRα1 antagonist α-BTx (0.1 μM) and was significantly reduced in cells after nAChRα1 silencing ($n = 5, p < 0.05$) (Fig. 7*b*). Preblocking with either α-BTx (0.1 μM) (data not shown) or *d*-TC (1.5×10^{-8} to 1.5×10^{-2} M) completely abrogated the binding of uPA (2.4×10^{-8} M) to nAChRα1 on the *uPAR*$^{-/-}$ fibroblasts. The concentration of *d*-TC that gave 50% inhibition (IC_{50}) was calculated to be 1.9 μM, a number similar to previously reported IC_{50} (2 μM) of the ACh-nAChRα1 binding (37) (Fig. 7*c*). In the nicotine binding assay (Fig. 7*d*), [^{3}H]nicotine bound to the *uPAR*$^{-/-}$ fibroblasts in a single binding site, yielding a K_d value of 31 nM. The nicotine binding was competitively inhibited by 15 μM *d*-TC blocking, with a predominant downward shift of the binding curve (20% reduction in maximum binding) but no apparent change in receptor affinity ($K_d = 30$ nM), suggesting that muscle-type nicotinic receptor mostly mediates the nicotine binding in kidney fibroblasts. The uPA (10^{-7} M) pre-exposure almost completely inhibited the specific binding of nicotine, supporting a competitive interaction between nicotine and uPA. These data indicate that uPA is a specific ligand for the muscle-type nicotinic receptor in kidney fibroblasts.

Urokinase Activates Fibroblast nAChRα1 Receptor Signaling by Tyrosine Phosphorylation—The next series of experiments was designed to identify key components of the uPA-nAChRα1 ligand-receptor signaling pathway in fibroblasts. The uPA-nAChRα1 ligation induced a significant cellular signaling response that was characterized by rapid protein tyrosine phosphorylation in uPAR-null fibroblasts (Fig. 8*a*). To determine if the nAChRα1 mediates this specific uPA-activated intracellular tyrosine phosphorylation signaling by receptor autophosphorylation, nAChRα1 responses to uPA stimulation were examined using co-IP and nAChRα1-silencing studies. Incubating uPAR-null renal fibroblasts with 2.4 ×

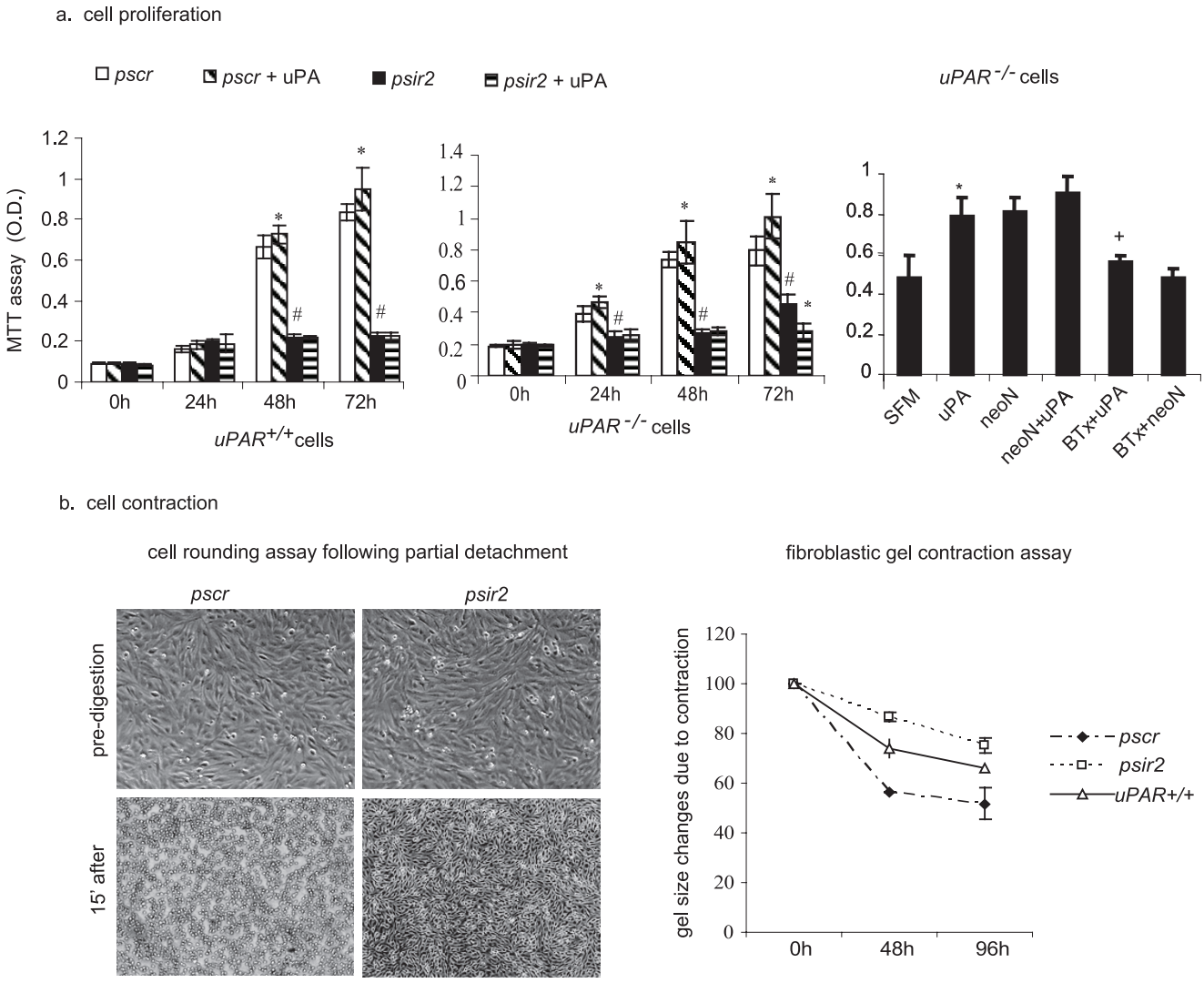

FIGURE 6. **Effects of nAChRα1-uPA interactions on fibroblast growth and matrix contraction.** *a*, cell proliferation assays detect a significant increase in the number of $uPAR^{+/+}$ and $uPAR^{-/-}$ fibroblasts at 48 and 72 h in the presence of uPA (2.4×10^{-8} M). nAChRα1 silencing with *psir2* significantly suppressed uPA stimulated proliferation in both $uPAR^{+/+}$ and $uPAR^{-/-}$ fibroblasts. *, $p < 0.05$, uPA^{+} *versus* media alone, $n = 10$; #, $p < 0.05$, *psir2 versus pscr*, $n = 10$. The uPA stimulated $uPAR^{-/-}$ cell growth was abrogated by the nAChRα1 antagonist αBTx (0.1 μM). +, $p < 0.05$, uPA *versus* uPA + BTx, $n = 10$. *b*, phase-contrast photomicrographs of kidney fibroblast cultures before and 15 min after treatment with cell detachment (digestion) buffer. Cells spontaneously contract (rounding) upon partial detachment. In routine cell detachment, it takes significantly (2-fold) longer for nAChRα1-silenced $uPAR^{-/-}$ fibroblast cells to become round compared with the non-silenced cells. Magnification was ×100. $n = 3$, two independent experiments. On the *right*, the graph represents the results of a more accurate collagen gel contraction assay using $uPAR^{-/-}$ kidney fibroblasts. The nAChRα1 silencing (*psir2*) significantly reduced fibroblastic gel contraction compared with scrambled siRNA treatment (*pscr*) ($n = 3$, two independent experiments). Wild-type ($uPAR^{+/+}$) cells that weakly express both uPAR and nAChRα1 receptors have an intermediate contractility.

10^{-8} M of uPA induced muscle-type nAChR tyrosine phosphorylation within 2 min; it rapidly dephosphorylated thereafter (Fig. 8*b*). This event was inhibited in the presence of α-BTx. On the other hand, nAChRα1 silencing in the uPAR-null fibroblasts completely suppressed both the base-line level of tyrosine phosphorylation and its transient response to the uPA stimulation (Figs. 8*c*). In order to further identify these signaling components, the phosphotyrosine proteins generated after uPAR-null fibroblasts were stimulated by uPA were enriched by IP and separated as two major visible bands in a non-reducing SDS gel (Fig. 8*d*). Mass spectrometry proteomic analysis of these two bands (in three independent sets of experiments) identified a group of proteins that might be involved in a specific signaling pathway involving calcium-binding proteins AHNAK and annexin 2, a cytoskeletal complex "*α-actinin-actin* + *vimentin-myosin*," and the nucleoprotein histone 4 (Fig. 8*e*). Selected key components of this signaling pathway were confirmed by co-IP experiments, including the receptor nAChRα1 and vimentin (Fig. 8*f*). These proteins showed different signaling responses in cells expressing nAChRα1 alone, uPAR alone, or both receptors (wild type), suggesting possible cross-talk between the two uPA receptors.

Urokinase Activates nAChRα1-mediated Calcium Signaling in Renal Fibroblasts—Since muscle-type nAChR is known to function as a ligand-gated calcium channel and given that several calcium-binding molecules and cytoskeleton proteins were identified in this study as tyrosine-phosphorylated following uPA ligation, the possibility that uPA might regulate nAChRα1 calcium channel function was examined. Upon uPA ligation, muscle-type nAChR functioned as an ion channel, leading to a

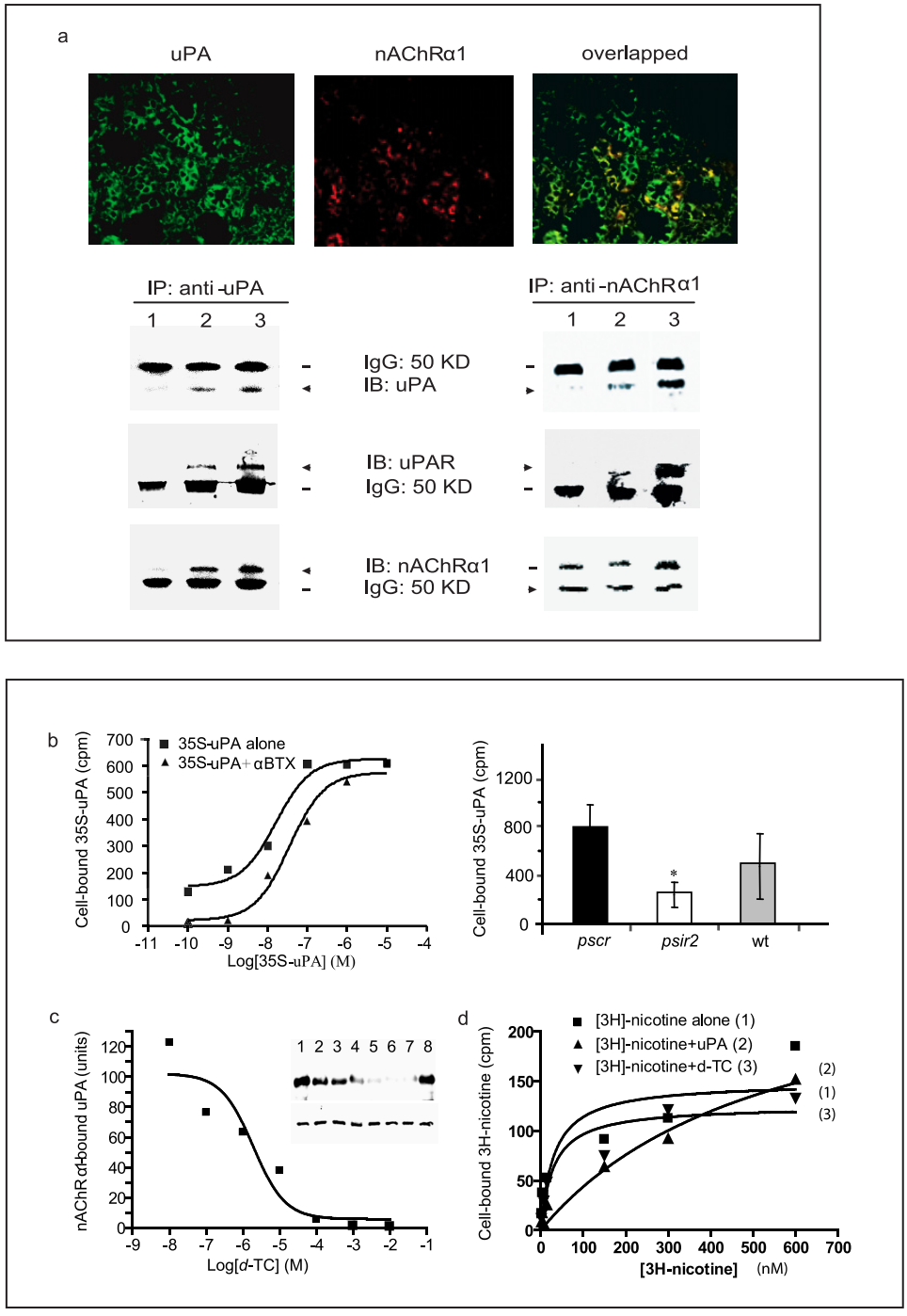

FIGURE 7. **Urokinase is a specific ligand of the nicotinic receptor nAChRα1.** *a*, double immunofluorescence staining illustrates renal tubular interstitial cells that co-express (*yellow overlap image*) nAChRα1 (*red*) and uPA (*green*) 7 days after UUO. Original magnification was ×250. uPA binding to both nAChRα1 and uPAR in normal and obstructed (UUO) kidneys, revealed by two-way IP-IB studies (IP with anti-uPA antibody and IB with anti-nAChRα1 antibody, or vice versa). *Lane 1*, uPA$^{-/-}$, 7-day UUO; *lane 2*, WT, sham; *lane 3*, WT, 7-day UUO. *b*, in a uPA-binding assay, ^{35}S-labeled uPA bound to uPAR-null kidney fibroblasts with a $K_d = 1.6 \times 10^{-8}$ M. That the binding is mediated specifically via nAChRα1 is evidenced by the right shift of the binding curve when exposed simultaneously to the receptor inhibitor αBTx (0.1 μM) and by significantly reduced binding when the nAChRα1 gene was silenced ($n = 5$; *, $p < 0.05$, *psir2* (silencing) *versus pscr* (scrambled); two independent experiments). *c*, preblocking with *d*-TC competitively inhibited uPA binding to uPAR-null fibroblasts, as measured using a co-IP approach. Illustrated is a representative uPA immunoblot (of two separate experiments) performed using fibroblast proteins immunoprecipitated with an anti-nAChRα1 antibody after the cells were incubated with biotinylated uPA (2.4×10^{-8} M) alone for 60 min at room temperature (shown in *lane 8*) or after a 30-min preincubation with increasing concentrations of *d*-TC (1.5×10^{-8} to 1.5×10^{-2} M), followed by the uPA exposure (*lanes 1–7*, represented in the *graph* by *black rectangles*). The *lower bands* were probed for β-actin, which served as a protein loading control. The calculated IC_{50} is 1.93 μM. *d*, [^{3}H]nicotine binding assays. 15 μM *d*-TC (a known muscle type nAChR antagonist) shifted the binding curve downward apparently; 10^{-7} M of uPA almost completely abrogated the specific nicotine binding, resulting in a nearly linear curve (nonspecific binding). Nicotine concentrations from 1.8 to 600 nM were used for these studies. Samples of each dosage were triplicate. Nonspecific background binding was subtracted from total binding. The data were best fit to a one-site model with a K_d = 31, 550, or 30 nM for *curve 1*, *2*, or *3*, respectively.

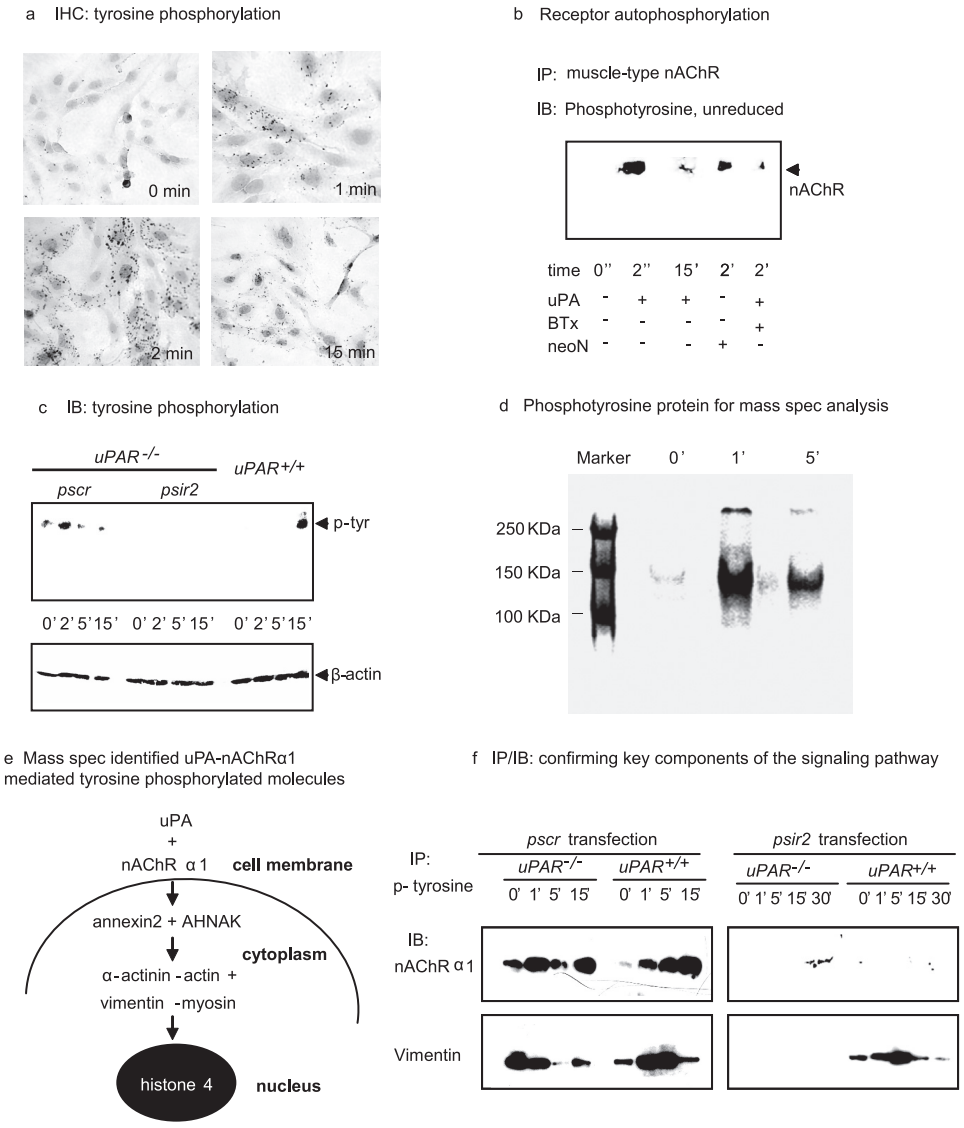

FIGURE 8. **The uPA-induced, nAChRα1-mediated tyrosine phosphorylation.** *a*, IHC photomicrograph of $uPAR^{-/-}$ kidney fibroblasts stained with an anti-phosphotyrosine antibody after uPA (2.4×10^{-8} M) stimulation illustrates cellular staining within minutes, suggesting intracellular signal transduction. Original magnification was ×250. *b*, IP with an anti-nAChR antibody followed by phosphotyrosine IB identifies phosphorylated proteins in $uPAR^{-/-}$ fibroblasts stimulated with uPA (representative blot from two independent experiments). neoN (1 nM) is a positive control. αBTx (0.1 μM) is the receptor inhibitor. *c*, IB illustrating the absence of uPA-induced tyrosine phosphorylation in the $uPAR^{-/-}$ fibroblasts following nAChRα1 silencing. *d*, SDS-PAGE identifies two major bands of immunoprecipitated tyrosine-phosphorylated proteins that were isolated from $uPAR^{-/-}$ fibroblasts after uPA stimulation. *e*, schematic summary of the tyrosine-phosphorylated signaling molecules that were identified by mass spectrometric analyses of proteins isolated from the gel illustrated in *d*. *f*, two selected components of the signaling complex were further characterized by IP/IB studies. The phospho-signaling molecules activated by the nAChRα1 alone ($uPAR^{-/-}$ cells + *pscr*) differed from those activated when both receptors ($uPAR^{+/+}$ cells + *pscr*) were expressed or when uPAR was alone ($uPAR^{+/+}$ cells + *psir2*). Lack of both receptors in *psir2*-treated $uPAR^{-/-}$ cells almost completely abrogated phosphotyrosine signaling.

1.6-fold increase in intracellular calcium levels $[Ca^{2+}]_i$ in the uPAR-null cells, as evaluated by fura-2 calcium measurements (Fig. 9*a*). The $[Ca^{2+}]_i$ responses of nAChRα1-silenced cells were significantly suppressed ($n = 3, p < 0.05$; two independent studies in each technical method). Whole cell patch clamp experiments were performed on the renal fibroblasts to examine the electrophysiological consequence of the uPA-nAChRα1 ligation-induced calcium mobilization. The whole cell current recordings in patch clamp studies in Fig. 9*b* illustrate examples of membrane currents elicited by 2.4×10^{-8} M of uPA. The access of uPA to intact cells elicited significant inward currents in WT or uPAR-null cells expressing high nAChRα1 levels (*pscr*), but not in uPAR-null nAChRα1-silenced cells (*psir2*). The uPA-elicited current responses of the uPAR-null cells were greatly diminished when the cells were preincubated with 1.5×10^{-5} M of *d*-TC 10 min prior to the uPA exposure (Fig. 9*b*, *b.2*).

The uPA-nAChRα1 Controls a Group of Fibrotic Genes in Cultured Fibroblasts—In order to probe the role of uPA-nAChRα1 receptor pathway in fibroblast gene expression, uPA-stimulated global gene expression responses in nAChRα1-expressing uPAR-null fibroblasts ("gene on" cells treated with *pscr*) were compared with the nAChRα1-silenced uPAR-null fibroblasts ("gene off" cells treated with *psir2*) (Fig. 9*c*). With the nAChRα1 "gene on," there were nine genes significantly up-regulated and 23 genes down-regulated in response to uPA stimulation ($n = 5, p < 0.0001$, -fold change >2.5, uPA-stimulated *versus* unstimulated) (listed in supplemental Tables S1 and S2). When the nAChRα1 gene was silenced ("gene off"), no gene was differentially expressed in response to uPA stimulation (only genes with -fold change of >2.5 and $p < 0.0001$ will be considered statistically significant). The uPA-nAChRα1 interaction induced the expression of a group of genes that are known to be involved in calcium signaling (*cdh11* (cadherin 11), *cnn3* (calponin 3), and *dpysl3* (dihydropyrimidinase-like 3)) and inflammatory-fibrotic response pathways (*col3α1* (procollagen III α1), *nelf* (nasal embryonic luteinizing hormone-releasing hormone factor, an FGF-2 downstream signaling molecule), and *YB-1* (Y box protein 1, a transcription factor)) (supplemental Table S1). These data demonstrate that the uPA-nAChRα1 interaction regulates the expression of a unique group of genes that may determine renal fibroblast phenotype.

DISCUSSION

The findings of the present study establish the α1 chain of the muscle type nicotinic acetylcholine receptor (nAChRα1) as a functional uPA receptor that is expressed by kidney fibroblasts. *In vivo* data are consistent with the hypothesis that uPA can

serve as a signaling ligand for nAChRα1 that is expressed *de novo* by (myo)fibroblasts that populate the interstitial area when kidneys are chronically injured. The uPA-nAChRα1 interaction can stimulate fibroblast proliferation and contraction. The nAChRα1 silencing in the UUO model of chronic kidney disease was associated with fibrosis attenuation and bet-

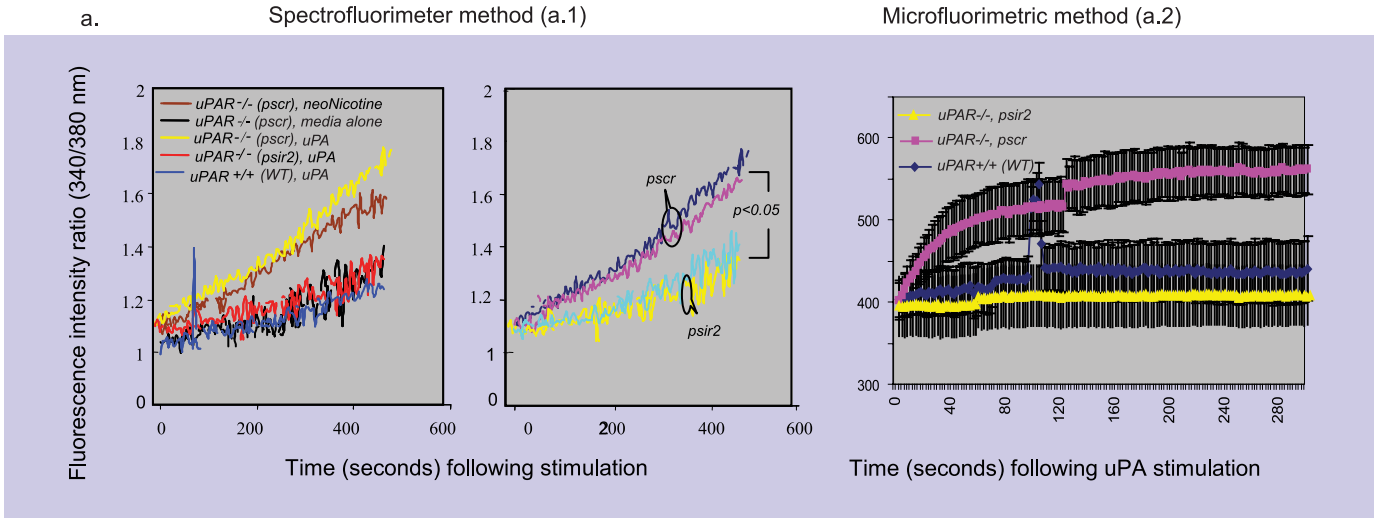

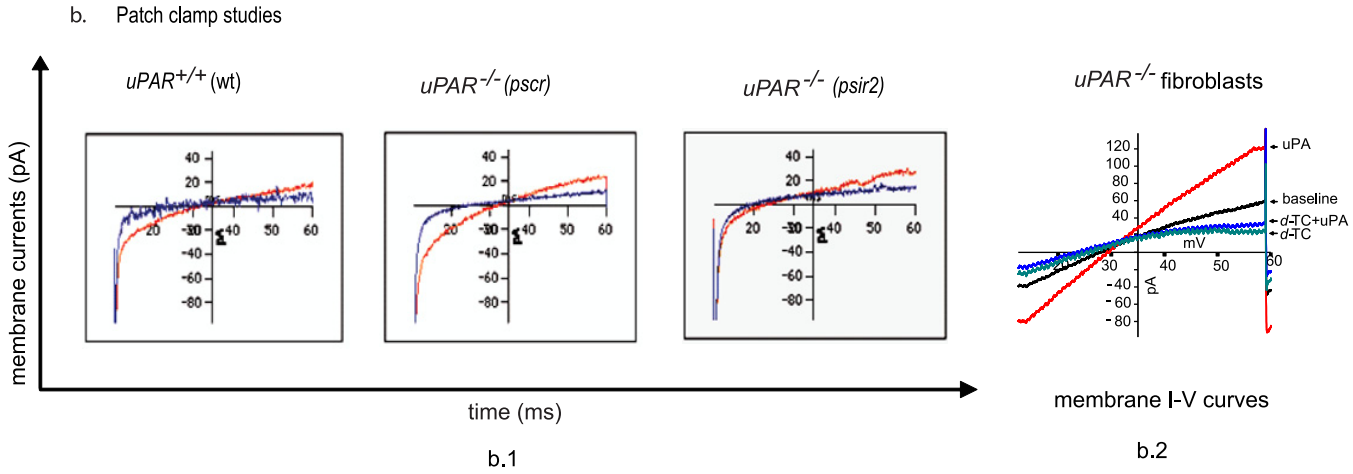

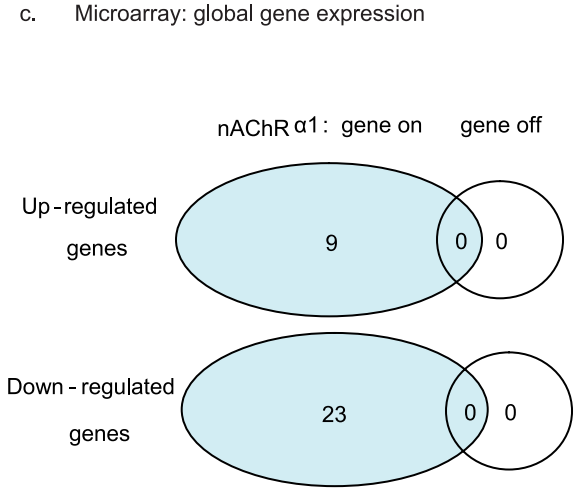

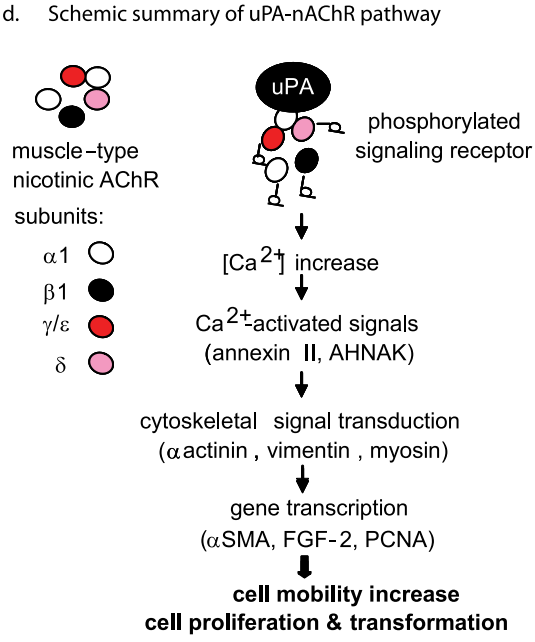

ter preservation of tubular cell integrity. This study further identified a series of intracellular signaling molecules and target genes that were regulated by this specific uPA ligand-receptor interaction. Given the diverse functions of the uPA serine protease system and the potential for uPA and nAChRα1 co-expression in other pathological conditions (2, 19, 24), our findings raise the possibility of similar functional interactions in other disease states.

The nAChRα1 is normally expressed at neuromuscular junctions as the ligand-binding subunits of the pentameric muscle-type nicotinic receptor $(\alpha1)_2\beta1\gamma\delta$ (fetal type) or $(\alpha1)_2\beta1\epsilon\delta$ (adult type) (19). The presence of different non-α subunits determines the binding affinity of the two α1 sites. Acetylcholine is the only previously known endogenous ligand for nAChRα1, with nicotine being an exogenous ligand in tobacco users. Based on estimates of dissociation constants (K_d) or 50% inhibiting concentration (IC_{50}) by *d*-TC, uPA binds with a 5–10-fold lower affinity to nAChRα1 than uPAR (44), but it is similar to the nicotine-nAChRα1 or ACh-nAChRα1 binding (37, 45). Beyond the neuromuscular junctions, nAChRα1 expression during pathological conditions has not been extensively investigated. *De novo* expression has been reported in a number of other tissues, including airway fibroblasts and epithelial cells, brain tissue from tobacco smokers, and non-small cell lung cancer cells (24). Normal kidneys, which produce large quantities of uPA, strongly express the nAChRα1. This study has demonstrated up-regulated nAChRα1 expression on renal interstitial fibroblasts (myofibroblasts) during fibrogenesis, whereas tubular and glomerular expression is down-regulated. Myofibroblast nAChRα1 expression appears to be uPA-dependent, since it disappears in the uPA-null mice. Our *in vitro* data further suggest that uPA stimulates fibroblastic nAChRα1 expression.

Myofibroblasts are characterized by their acquisition of myocyte characteristics, such as contractile properties and αSMA expression. They are more profibrotic than resting fibroblasts and are thought to be the primary source of the scar-forming extracellular matrix proteins in many solid organs, including kidneys (41, 44). The molecular basis of renal myofibroblast accumulation remains incompletely understood. Growth factors, such as transforming growth factor-β, FGF-2, platelet-derived growth factors, and members of the urokinase system, have been shown to participate (26, 31, 44). The current study has shown that uPA can initiate fibroblast nAChRα1 signaling by opening calcium channels and by activating tyrosine phosphorylation signals to stimulate their proliferation, contraction, and phenotypic transformation (Fig. 9*d*).

An important question we have attempted to address in this study is whether uPA is the major pathological ligand for nAChRα1 *in vivo* in the kidney. Although receptor-bound ACh levels increased after UUO, the protein localized to glomeruli and tubules, whereas interstitial expression was not detected. Although the possibility that kidney-derived ACh plays a role cannot be excluded, cell-specific effects would be predicted, and interaction with interstitial myofibroblasts is less likely based on our immunolocalization data. Previous studies suggest that ACh also binds to another kidney receptor, the nAChRα7, which exerts an anti-inflammatory effect (46).

The uPA and nAChRα1 proteins co-localize mainly to interstitial cells of chronically damaged kidneys. A physical association between uPA and nAChRα1 *in vivo* is supported by the fact that the two proteins can be co-immunoprecipitated from kidney tissue. The signaling function of uPA interacting with nAChRα1 was demonstrated by *in vitro* studies using kidney fibroblasts. The net effect was an increase in fibroblast numbers and phenotypic changes associated with scarring: αSMA expression and increased matrix gel contraction. The identified downstream phosphoprotein signals, including calcium-binding proteins (AHNAK and annexin 2) and cytoskeletal proteins (α-actinin, actin, vimentin, and myosin), appear relevant to the myofibroblast phenotype and functions in fibrosis (47, 48). FGF-2 is a key autocrine cytokine that mediates fibroblast proliferation during renal fibrogenesis (49). That uPA-nAChRα1 interaction significantly up-regulated (>5-fold increase) fibroblastic Nelf (a downstream signal of FGF-2) and Col3 α1 gene expression *in vitro* (as indicated by microarray studies) supports our *in vivo* finding of more robust renal FGF-2 expression, fibroblast proliferation, and total collagen accumulation in the non-silenced wild-type mice compared with the nAChRα1-silenced mice.

Our previous studies in uPA and uPAR genetically engineered mice found that, unlike nAChRα1, uPAR is up-regulated in both tubules and interstitial cells during UUO and functions to inhibit myofibroblast recruitment and fibrosis severity (30, 31). Furthermore, the net effect of endogenous uPA deficiency was neutral with respect to fibrosis severity (50).

FIGURE 9. **Calcium signaling and genes regulated by uPA-nAChRα1 interaction.** *a*, calcium influx studies. Fibroblast monolayers were preloaded with fura 2-AM. $[Ca^{2+}]_i$ was measured following the addition of uPA either using harvested cell suspensions (*a.1*) or directly onto individual cell monolayers (*a.2*). A significant $[Ca^{2+}]_i$ spike was stimulated shortly after adding uPA to $uPAR^{-/-}$ cells that endogenously overexpress muscle-type nAChR (*pscr*), but not in $uPAR^{+/+}$ cells or nAChRα1-silenced $uPAR^{-/-}$ cells (*psir2*). Treatment with neoN (1 nM) induced a similar $[Ca^{2+}]_i$ spike response in the $uPAR^{-/-}$ (*pscr*) cells. The addition of media alone served as a non-stimulated negative control. For both studies, $n = 3$; $p < 0.05$, *psir2 versus pscr*. The *x* axis shows the survey duration following stimulation (seconds); the *y* axis shows the 500 nm fluorescence intensity ratio when excited at 340/380 nm. *b*, by patch clamp studies, uPA (2.4×10^{-8} M) stimulates the receptor to function as an ion channel, resulting in a significant inward current in fibroblasts. The *x* axis is 50-ms voltage ramp spinning the voltage range from −100 mV to +100 mV. The *y* axis shows the recorded membrane currents (pA). In *b.1*, the *blue line* represents base-line currents before uPA stimulation. The *red line* represents inward currents elicited by uPA. Recording began 15 s after uPA stimulation. *WT*, wild-type $uPAR^{+/+}$ fibroblasts; *pscr*, $uPAR^{-/-}$ cells naturally overexpressing nAChRα1 (transfected with *pscr*); *psir2*, $uPAR^{-/-}$ cells with nAChRα1 silenced (with *psir2*). In *b.2*, the *I-V* curves were recoded in $uPAR^{-/-}$ cells before (base line) and after uPA stimulation. Preincubation with *d*-TC (1.5×10^{-5} M) for 10 min prevented uPA-elicited current responses. *c*, schematic summary of the results of microarray studies. The uPA-nAChRα1 interaction regulated the expression of 32 genes that are identified in supplemental Tables S1 and S2. *d*, schematic summary of potential signal transduction pathways and cellular effects initiated by uPA-nAChRα1 ligation. The receptor is formed by the assembly of five subunits: $(\alpha1)_2\beta1\gamma\delta$ (fetal type) or $(\alpha1)_2\beta1\epsilon\delta$ (adult type). The two α1 subunits are involved in shaping the ligand-binding sites. Binding of uPA to α_γ and α_δ sites induces conformational changes that lead to channel opening. The influx of calcium and increase in the cytosolic concentration of calcium ions ($[Ca^{2+}]_i$) transmit information via a cytoskeletal signaling transduction pathway that is crucial for fibroblastic motility. The muscle-type nAChR function is regulated by receptor tyrosine phosphorylation upon ligation. These signals stimulate the cells to initiate the transcriptions of genes that promote cell proliferation and transformation.

Taken together with the findings in the present study, it is evident that uPA is a complex ligand with the potential for diverse cellular effects that are receptor-dependent. Remarkably, the uPA-nAChRα1 and the uPA-uPAR pathways have opposite effects on kidney fibrosis. Specifically targeting the fibroblastic uPA-nAChRα1 pathway was beneficial in an experimental model of chronic kidney disease. It is tempting to speculate that this pathway is a viable pharmaceutical target to inhibit fibroblastic activation and kidney fibrosis. The biological significance of our finding may be relevant to disorders that extend beyond chronic kidney disease.

Acknowledgments—We acknowledge support from Dr. Andrew M. Scharenberg (Department of Immunology, University of Washington) for providing insightful advice and instruments for patch clamp studies, Dr. Ping Liu from Dr. Scharenberg's laboratory for technical assistance in calcium measurements, Dr. Neil M. Nathanson (Department of Pharmacology, University of Washington) for important advice on designing the urokinase receptor binding assays, and Liping Cheng (Seattle Children's Research Institute) for technical support in binding assays. The microarray gene expression studies were performed in Center for Array Technologies (University of Washington). The mass spectrometry work was done in the Proteomics Core facility of the Fred Hutchinson Cancer Research Center (Seattle, WA). We thank the Seattle Biomedical Research Institute for participating in DNA sequencing to confirm the plasmid reconstructions.

REFERENCES

1. Astrup, T., and Sterndorff, I. (1955) *Scand. J. Clin. Lab. Invest.* **7,** 239–245
2. Zhang, G., and Eddy, A. A. (2008) *Front. Biosci.* **13,** 5462–5478
3. du Toit, P. J., Van Aswegen, C. H., Steinmann, C. M., Klue, L., and Du Plessis, D. J. (1997) *Med. Hypotheses* **49,** 57–59
4. Jin, T., Bokarewa, M., and Tarkowski, A. (2005) *J. Infect. Dis.* **192,** 429–437
5. Steins, M. B., Padró, T., Schwaenen, C., Ruiz, S., Mesters, R. M., Berdel, W. E., and Kienast, J. (2004) *Blood Coagul. Fibrinolysis* **15,** 383–391
6. Killeen, S., Hennessey, A., El Hassan, Y., and Waldron, B. (2008) *Drug News Perspect.* **21,** 107–116
7. Brommer, E. J., Van den Wall Bake, A. W., Dooijewaard, G., van Loon, B. J., Emeis, J. J., and Weening, J. J. (1994) *Thromb. Haemost.* **71,** 19–25
8. Pawlak, K., Pawlak, D., and Mysliwiec, M. (2007) *Thromb. Res.* **120,** 871–876
9. Vassalli, J. D., Baccino, D., and Belin, D. (1985) *J. Cell Biol.* **100,** 86–92
10. Mondino, A., and Blasi, F. (2004) *Trends Immunol.* **25,** 450–455
11. Annecke, K., Schmitt, M., Euler, U., Zerm, M., Paepke, D., Paepke, S., von Minckwitz, G., Thomssen, C., and Harbeck, N. (2008) *Adv. Clin. Chem.* **45,** 31–45
12. Stempien-Otero, A., Plawman, A., Meznarich, J., Dyamenahalli, T., Otsuka, G., and Dichek, D. A. (2006) *J. Biol. Chem.* **281,** 15345–15351
13. Koopman, J. L., Slomp, J., de Bart, A. C., Quax, P. H., and Verheijen, J. H. (1998) *J. Biol. Chem.* **273,** 33267–33272
14. Mukhina, S., Stepanova, V., Traktouev, D., Poliakov, A., Beabealashvilly, R., Gursky, Y., Minashkin, M., Shevelev, A., and Tkachuk, V. (2000) *J. Biol. Chem.* **275,** 16450–16458
15. Poliakov, A. A., Mukhina, S. A., Traktouev, D. O., Bibilashvily, R. S., Gursky, Y. G., Minashkin, M. M., Stepanova, V. V., and Tkachuk, V. A. (1999) *J. Recept. Signal Transduct. Res.* **19,** 939–951
16. Zhang, G., Cai, X., López-Guisa, J. M., Collins, S. J., and Eddy, A. A. (2004) *J. Am. Soc. Nephrol.* **15,** 2090–2102
17. Liang, O. D., Chavakis, T., Linder, M., Bdeir, K., Kuo, A., and Preissner, K. T. (2003) *Biol. Chem.* **384,** 229–236
18. Franco, P., Vocca, I., Carriero, M. V., Alfano, D., Cito, L., Longanesi-Cattani, I., Grieco, P., Ossowski, L., and Stoppelli, M. P. (2006) *J. Cell Sci.* **119,** 3424–3434
19. Kalamida, D., Poulas, K., Avramopoulou, V., Fostieri, E., Lagoumintzis, G., Lazaridis, K., Sideri, A., Zouridakis, M., and Tzartos, S. J. (2007) *FEBS J.* **274,** 3799–3845
20. Cauley, K, Agranoff, B. W., and Goldman, D. (1989) *J. Cell Biol.* **108,** 637–645
21. Ploug, M., and Ellis, V. (1994) *FEBS Lett.* **349,** 163–168
22. Miles, K., Audigier, S. S., Greengard, P., and Huganir, R. L. (1994) *J. Neurosci.* **14,** 3271–3279
23. Wang, X. M., Tsay, H. J., and Schmidt, J. (1990) *EMBO J.* **9,** 783–790
24. Carlisle, D. L., Hopkins, T. M., Gaither-Davis, A., Silhanek, M. J., Luketich, J. D., Christie, N. A., and Siegfried, J. M. (2004) *Respir. Res.* **5,** 27–43
25. Gou, D., Jin, N., and Liu, L. (2003) *FEBS Lett.* **548,** 113–118
26. Zhang, G., Kernan, K. A., Collins, S. J., Cai, X., López-Guisa, J. M., Degen, J. L., Shvil, Y., and Eddy, A. A. (2007) *J. Am. Soc. Nephrol.* **18,** 846–859
27. Zhang, G., Budker, V., and Wolff, J. A. (1999) *Hum. Gene Ther.* **10,** 1735–1737
28. Dai, C., Yang, J., and Liu, Y. (2002) *J. Am. Soc. Nephrol.* **13,** 411–422
29. Carmeliet, P., Schoonjans, L., Kieckens, L., Ream, B., Degen, J., Bronson, R., De Vos, R., van den Oord, J. J., Collen, D., and Mulligan R. C. (1994) *Nature* **368,** 419–424
30. Zhang, G., Kim, H., Cai, X., Lopez-Guisa, J. M., Carmeliet, P., and Eddy, A. A. (2003) *J. Am. Soc. Nephrol.* **14,** 1234–1253
31. Zhang, G., Kim, H., Cai, X., López-Guisa, J. M., Alpers, C. E., Liu, Y., Carmeliet, P., and Eddy, A. A. (2003) *J. Am. Soc. Nephrol.* **14,** 1254–1271
32. Kivirikko, K. I., Laitinen, O., and Prockop, D. J. (1967) *Anal. Biochem.* **19,** 249–255
33. Asanuma, K., Yanagida-Asanuma, E., Faul, C., Tomino, Y., Kim, K., and Mundel, P. (2006) *Nat. Cell Biol.* **8,** 485–491
34. Lengronne, A., Pasero, P., Bensimon, A., and Schwob, E. (2001) *Nucleic Acids Res.* **29,** 1433–1442
35. Montesano, R., and Orci, L. (1988) *Proc. Natl. Acad. Sci. U.S.A.* **85,** 4894–4897
36. Mazzieri, R., D'Alessio, S., Kenmoe, R. K., Ossowski, L., and Blasi, F. (2006) *Mol. Biol. Cell* **17,** 367–378
37. Carlin, B. E., Lawrence, J. C., Jr., Lindstrom, J. M., and Merlie, J. P. (1986) *Proc. Natl. Acad. Sci. U.S.A.* **83,** 498–502
38. Duner, E., Di Virgilio, F., Trevisan, R., Cipollina, M. R., Crepaldi, G., and Nosadini, R. (1997) *Hypertension* **29,** 1007–1013
39. Akk, G., and Steinbach, J. H. (2003) *J. Physiol.* **551,** 155–168
40. Matsuo, S., López-Guisa, J. M., Cai, X., Okamura, D. M., Alpers, C. E., Bumgarner, R. E., Peters, M. A., Zhang, G., and Eddy, A. A. (2005) *Kidney Int.* **67,** 2221–2238
41. Eyden, B. (2005) *J. Submicrosc. Cytol. Pathol.* **37,** 109–204
42. Plekhanova, O. S., Stepanova, V. V., Ratner, E. I., Bobik, A., Tkachuk, V. A., and Parfyonova, Y. V. (2006) *J. Vasc. Res.* **43,** 437–446
43. Pang, I. H., Shade, D. L., Tamm, E., and DeSantis, L. (1993) *Invest. Ophthalmol. Vis. Sci.* **34,** 1876–1879
44. Eddy, A. A. (2005) *Adv. Chronic Kidney Dis.* **12,** 353–365
45. Morgan, D., Parsons, M. E., and Whelan, C. J. (2001) *Biochem. Pharmacol.* **61,** 733–740
46. Yeboah, M. M., Xue, X., Duan, B., Ochani, M., Tracey, K. J., Susin, M., and Metz, C. N. (2008) *Kidney Int.* **74,** 62–69
47. Lee, I. H., Lim, H. J., Yoon, S., Seong, J. K., Bae, D. S., Rhee, S. G., and Bae, Y. S. (2008) *J. Biol. Chem.* **283,** 6312–6320
48. Chaurasia, S. S., Kaur, H., de Medeiros, F. W., Smith, S. D., and Wilson, S. E. (2009) *Exp. Eye Res.* **89,** 133–139
49. Strutz, F., Zeisberg, M., Hemmerlein, B., Sattler, B., Hummel, K., Becker, V., and Müller, G. A. (2000) *Kidney Int.* **57,** 1521–1538
50. Yamaguchi, I., López-Guisa, J. M., Cai, X., Collins, S. J., Okamura, D. M., and Eddy, A. A. (2007) *Am. J. Physiol. Renal Physiol.* **293,** F12–F19